GRAPHICAL ABSTRACT

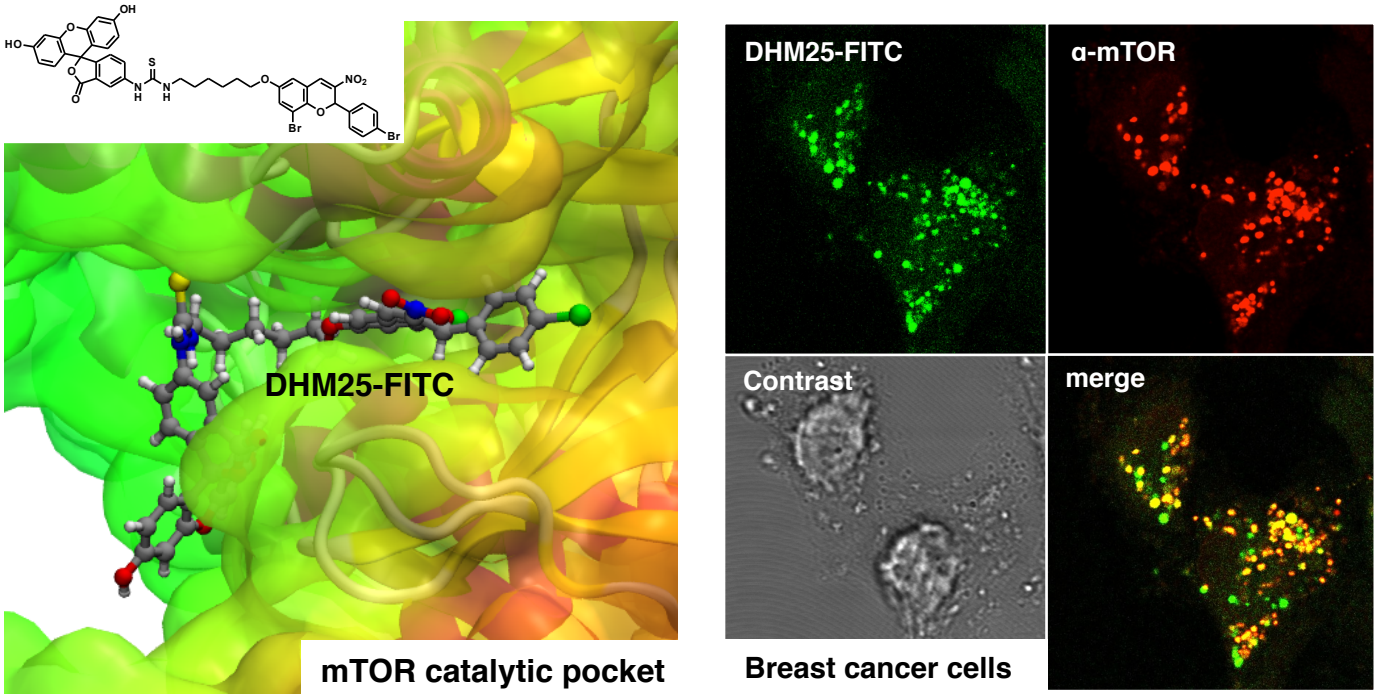

A novel covalent mTOR inhibitor, DHM25, shows *in vivo* anti-tumor activity against triple-negative breast cancer cells

Amélie Fouqué,[1,2,3] Olivier Delalande,[1,4] Mickael Jean,[1,5] Rémy Castellano,[6] Emmanuelle Josselin,[6] Marine Malleter,[1] Kenji F. Shoji,[1,7] Mac Dinh Hung,[8] Hariniaina Rampanarivo,[1,2,3,4] Yves Collette,[6] Pierre van de Weghe,[1,5,9,*] and Patrick Legembre[1,2,3,9,*]

[1]Université de Rennes-1, 2 avenue du Prof. Leon Bernard, 35043 Rennes, France

[2]CLCC Eugène Marquis, INSERM ER440 Oncogenesis, Stress & Signaling, rue bataille Flandres Dunkerque, 35042 Rennes, France

[3]Equipe Labellisée Ligue Contre le Cancer, rue bataille Flandres Dunkerque, Rennes

[4]IGDR, CNRS UMR 6290, UFR des Sciences Biologiques et Pharmaceutiques, 2 Av. du Professeur Léon Bernard, 35043 Rennes, France

[5]UMR6226, CNRS, Institut des Sciences Chimiques de Rennes, Equipe Produits Naturels, Synthèses, Chimie Médicinale, UFR des Sciences Biologiques et Pharmaceutiques, 2 Av. du Professeur Léon Bernard, 35043 Rennes, France

[6]CRCM, INSERM, U1068; Institut Paoli-Calmettes; Aix-Marseille Université; CNRS, UMR 7258, Marseille, France

[7]INSERM, U1085, 2 avenue du Prof. Leon Bernard, 35043 Rennes, France

[8]Faculty of Chemistry, National Vietnam University, 19 Le Thanh Tong, Hanoi, Vietnam

Running title: Generation of a new mTOR inhibitor

Key Words: PI3K, mTOR, chromene, breast cancer, chemotherapy

The authors disclose no potential conflicts of interest.

ABSTRACT

Constitutive activation of the PI3K/mTOR signaling pathway contributes to carcinogenesis and metastasis in most, if not all, breast cancers. From a chromene backbone reported to inhibit class I PI3K catalytic subunits, several rounds of chemical syntheses led to the generation of a new collection of chromologs that showed enhanced ability to kill PI3K-addicted cancer cells and to inhibit Akt phosphorylation at serine 473, a hallmark of PI3K/mTOR activation. This initial screen uncovered a chromene designated DHM25 that exerted potent anti-tumor activity against breast tumor cell lines. Strikingly, DHM25 was shown to be a selective and covalent inhibitor of mTOR using biochemical and cellular analyses, modeling, and a large panel of kinase activity assays spanning the human kinome (243 kinases). Finally, *in vivo*, this novel drug was an efficient inhibitor of growth and metastasis of triple-negative breast cancer cells, paving the way for its clinical application in oncology.

INTRODUCTION

The PI3K/mTOR signaling pathway controls cell survival, growth, proliferation, differentiation, and motility. Therefore, it is not surprising to find this signaling pathway deregulated in human cancers. PI3K phosphorylates the D3 position on phosphoinositide to yield phosphatidylinositol-3,4,5-trisphosphate (PIP3). This phosphorylated lipid can then interact with several proteins containing a pleckstrin homology (PH) domain. Negative regulation of this pathway is mainly conferred by phosphatase and tensin homolog deleted on chromosome 10 (PTEN)[1, 2] and inositol polyphosphate-4-phosphatase (INPP4B),[3] which dephosphorylate PIP3 and PIP2, respectively. The serine/threonine kinase Akt possesses a PH domain, and its recruitment to the plasma membrane induces its activation through phosphorylation at threonine 308 by PDK1[4] and at serine 473 by mammalian target of rapamycin complex 2 (mTORC2).[5] Once activated, Akt phosphorylates and thereby inactivates tuberous sclerosis complex-2 (TSC2), a GTPase-activating protein (GAP) that inhibits the GTPase Rheb (RAS homolog expressed in brain).[6-8] The release of the TSC2-driven Rheb blockage leads to the activation of the serine-threonine kinase mTOR.[9] mTOR belongs to the PI3K-related kinase family and forms at least two complexes whose exhaustive composition, cellular distribution, and function remain to be defined. While mTOR complex 1 (mTORC1) is instrumental in translation and cell growth regulation via phosphorylation of substrates such as eukaryotic initiation factor eIF4E binding protein (4E-BP1), mTOR complex 2 (mTORC2) regulates a different set of substrates, including Akt.[10] Of interest, mTORC1 exerts a negative feedback loop on both PI3K and mTORC2[11, 12] and thereby downregulates Akt activity. Rapamycin, a macrolide [13] interacting with FKBP12, selectively inhibits mTORC1.[14-16] Despite promising results in animal models of cancer, rapamycin and rapalogs were generally disappointing in human trials (reviewed in [17]). One explanation for these disappointing results is that by eliminating the mTORC1-dependent negative feedback

program, rapalogs lead to prolonged activation of the mTORC2/Akt signaling pathway,[18] which may promote the occurrence of new cancers during chronic treatment. To overcome this limitation, ATP-competitive inhibitors that potently block both mTORC1 and mTORC2 are sought as anticancer agents.[19] Beyond rapalogs that show limited clinical benefit in cancers, few *N*-heterocyclic derivatives have been identified as mTOR inhibitors. These small molecules, AZD8055, NVP-BEZ235, OSI-027, INK128 and Torin1, inhibit both mTORC1 and mTORC2 and are currently in clinical trials.[20] Although these ATP-competitive inhibitors exert an anti-cancer activity, only NVP-BEZ235 presents some interest to treat breast cancer patients and may be used in combination with other chemotherapeutic drugs to improve clinical outcomes in this pathology (tested in phase I and II clinical trials, see on clinicaltrials.gov/). This deficiency of small inhibitors of the mTOR activity for the treatment of breast cancer reveals the urgent need for the development of new and potent compounds.

The most common cancers are colorectal cancers (13.6%) and breast cancers (13.1%).[21] Based on their gene expression profiles, breast cancers are categorized as luminal A/B, HER-2+, and basal-like, with a close relationship between this classification and the clinical outcome of the tumors.[22] Basal-like breast cancers are closely related to triple-negative breast cancers (TNBCs).[23] Representing 10–20% of all breast cancers, TNBC/basal-like tumors account for a disproportionate number of mortalities, in part due to their aggressiveness and the lack of effective therapeutic regimens. Indeed, while the estrogen receptor (ER)-positive cancers closely related to luminal A/B cancers receive hormone therapy[24] and HER2-amplified cancers are a clinical success because of neutralizing antibodies targeting HER2,[25] TNBCs can only be treated with chemotherapy.[26] A recent large-scale study of 50 luminal breast cancer genomes sequenced at high coverage identified over 1700 genic mutations, but only three of these genes were mutated at frequencies that approached or exceeded 10%.[27] Among these genes, *PIK3CA*, which codes for the p110α catalytic sub-unit of PI3K, harbored

mutations in 43% of the analyzed tumors.[27] Although PIK3CA mutations remain less frequent in TNBCs as compared to non-TNBCs, loss-of-function mutations or reduced expression of PTEN or INPP4B are detected in 67% and 53% of TNBCs, respectively,[28] confirming that deregulation of the PI3K/mTOR signaling pathway is a common event in breast carcinogenesis and supporting the need to develop potent and selective inhibitors of the PI3K/mTOR signaling pathway to treat this pathology.

From a chromene derivative showing a weak affinity for PI3K (IC_{50} of 10–50 μM for the different p110 catalytic subunits of PI3K),[29] we used cell-based, enzyme, and biochemical assays to generate a potent and irreversible mTOR inhibitor designated DHM25 [6,8-dibromo-2-(4-bromophenyl)-3-nitro-2*H*-chromene] that efficiently kills breast cancer cells.

RESULTS

Synthesis of chromene derivatives.

To develop new and potent PI3K inhibitors, a chromene backbone designated S14161/pichromene was selected for its ability to kill malignant cell lines by inhibiting all class I PI3K catalytic subunits.[29] Accordingly, a number of synthetic strategies have been described for the preparation of chromene derivatives. Among them, we sought to use an approach based on the addition of salicylaldehydes to α,β-unsaturated compounds promoted by organic bases. The utilization of small chiral organic molecules as metal-free catalysts, especially in the synthesis of pharmaceuticals was chosen because of the "green" advantage of not contaminating the final product with traces of heavy metals.[30-32] The chromene derivatives were synthesized using pipecolic acid or tetramethylguanidine as catalyst to promote the addition of various substituted salicylaldehydes to several α,β-unsaturated derivatives (Scheme 1). By varying first the west part of the pichromene and second the aryl group of the east part, several structural modifications were progressively undertaken until the generation of the two chromene derivatives, DHM9 and DHM25 (see below).

Selection of a potent PI3K inhibitor.

By modifying first the west part of the scaffold, new compounds were synthesized, and their ability to kill two PI3K-dependent leukemic T cell lines (CEM and Jurkat) was tested (Fig. S1A).[33, 34] To focus on compounds that were potentially selective for the PI3K signaling pathway, chromologs were selected that exerted more cytotoxic activity on CEM/Jurkat cells than on the leukemic T cell line H9, whose survival relies to a lesser extent on PI3K signaling (Fig. 1B).[34] This screening test highlighted that although pichromene was more efficient at killing CEM and Jurkat cells than the well-established and potent PI3K inhibitor wortmannin (Fig. S1A), it probably did not exert its cytotoxic effect by inhibiting the PI3K signaling

pathway, because CEM/Jurkat and H9 cells were killed to a similar extent (Fig. 1B-C). Although PWPHT45, PWPHT47, PWPHT88, PWPHT89, and PWPHT90 showed increased cytotoxic activity compared to pichromene (Fig. S1A), only PWPHT45 and PWPHT89 killed more efficiently CEM/Jurkat cells than H9 cells (Fig. 1B-C), indicating that these two chromene derivatives could exert their cytotoxic effect by selectively inhibiting the PI3K signaling pathway. To confirm this assumption, the ability of these chemicals to inhibit the PI3K signaling pathway in CEM cells (Fig. 1D) and in Jurkat cells (Fig. S1B) was next analyzed by assessing their impact on the phosphorylation of Akt, a downstream PI3K effector. Confirming the cell-based assay, incubation of CEM or Jurkat cells for 1 or 2 hours with pichromene (10 μM) did not reduce the level of Akt phosphorylation at serine 473 in (Fig. 1D and S1B), indicating that this compound was not a direct inhibitor of PI3K and that its cytotoxic activity on CEM and Jurkat cells likely occurred through a PI3K-independent mechanism. By contrast, chromene derivatives PWPHT33, PWPHT45, PWPHT47, PWPHT54, PWPHT52, PWPHT88, and PWPHT89 showed an inhibitory effect on Akt phosphorylation (Fig. 1D). PWPHT45 and PWPHT89 were, therefore, the most interesting backbones from this first set of chromologs and were subsequently used to design a second collection of derivatives (Fig. S2). The aryl substituents were modified in order to study the influence of various compounds with different electronic or lipophilic properties and steric hindrance on the cytotoxic activity of our lead compound. Among this second library, five derivatives displayed better cytotoxic activity toward the leukemic T cell line CEM than PWPHT45 and PWPHT89 (Fig. 1E). Next, DHM9, DHM10, and DHM25 were selected for their ability to inhibit Akt phosphorylation at serine 473 (Fig. 1F-I). Of note, DHM9 and DHM25 corresponded to PWPHT89 and PWPHT45 backbones, respectively, in which the fluoride atom was replaced by bromine. Finally, these three compounds exhibited an *in cellulo* IC_{50} of between 0.376 and 2.744 μM, whereas the PI3K inhibitor LY294002, which

shares some structural similarities with chromologs, showed an IC_{50} close to 100 μM in CEM cells (Fig. 1H-I). In summary, from a weak PI3K inhibitor (pichromene) and two cell-based/biochemical assays, two rounds of synthesis led to the identification of two novel chromologs (DHM9 and DHM25) showing dramatically improved PI3K inhibitory activity as compared to S14161/pichromene.

DHM9 and DHM25 efficiently kill breast tumor cells.

Because carcinogenesis in breast epithelial cells relies on the constitutive activation of the PI3K/mTOR signaling pathway, which occurs through the deregulation of various molecular mechanisms including down-regulation of PTEN activity and/or expression (see Fig. S3), constitutive activation of PI3K (gain-of-function mutations in *PIK3CA* or *PIK3R1* indicated in Fig.2A), or induction of the Ras signaling pathway, we next evaluated the cytotoxic effect of our leads on nine breast tumor cell lines covering all breast cancer sub-types and exhibiting deregulation of PI3K signaling through various molecular mechanisms (Fig. 2A). Independently of their histological classification (TNBC, non-TNBC, or $HER2^+$), all breast cancer cell lines exposed for 24 hours to the selected chromologs underwent a cell death program (Fig. 2A-B). Among the molecules tested, DHM25 and, to a lesser extent, DHM9 showed the most efficient cytotoxic activity (Fig. 2A). Because all breast malignant cells were sensitive to DHM25 treatment regardless of mutations in the PI3K signaling pathway, either these mutations did not affect the inhibitory capacity of DHM25, or DHM25 targeted a downstream protein in the PI3K signaling pathway.

DHM25 is a selective mTOR inhibitor.

To identify the molecular targets of DHM9 and DHM25, their inhibitory activity against 243 human protein kinases was evaluated using KinaseProfiler assay™. Strikingly, despite

structural similarities between DHM25 and DHM9 (only one additional bromine in position 8 of DHM25 as compared to DHM9), the KinaseProfiler assay™ revealed that different sets of kinases were targeted by DHM9 and DHM25 (Fig. 3A). More importantly, no PI3Ks were inhibited by DHM25 or DHM9. Indeed, while 1 μM DHM9 abrogated the activity of tyrosine (c-yes) and serine/threonine kinases (p70S6K, LOK, BrSK1, TSSK1, and NLK), the same concentration of DHM25 inhibited only mTOR activity (Fig. 3A). It is noteworthy that Akt phosphorylation at serine 473, the biochemical marker that we followed to determine the PI3K inhibitory effect of chromologs, is the direct target of mTORC2.[10, 35] To confirm that DHM25 was an mTOR inhibitor, its ability to inhibit the phosphorylation of mTORC1 and C2 substrates was evaluated. To this end, the phosphorylation status of 4E-BP1 (a direct substrate of mTORC1) and S6 (a substrate of p70S6K, another target of mTORC1) was monitored (Fig. 3B-C). DHM25 activity was also compared with that of rapamycin, an mTORC1 kinase inhibitor that exerts its activity by preventing its binding to FK506-binding protein of 12 kDa (FKBP12)[36] while sparing mTORC2 activity.[37, 38] While DHM25 exposure blocked Akt phosphorylation at serine 473 (IC_{50} = 1.5 μM), rapamycin treatment did not affect the intensity of phosphorylation of this mTORC2 substrate (Fig. 3B). By densitometry analysis, DHM25 exhibited a similar capacity to inhibit the phosphorylation of 4E-BP1 (IC_{50} = 8.3 μM) and S6 (IC_{50} = 1 μM). By contrast, 4E-BP1 phosphorylation was relatively resistant to rapamycin treatment (IC_{50} = 9.5 μM) compared to S6 phosphorylation (IC_{50} = 0.3 nM). A recent study demonstrated that the difference in rapamycin sensitivity between these two mTORC1 substrates was dependent on their different affinities for the mTORC1 kinase domain.[39] Indeed, p70S6K activity was more sensitive to rapamycin treatment because of its weaker affinity for mTORC1 as compared to 4E-BP1.[39] The differential inhibitory effects of rapamycin on 4E-BP1 and S6 contrasted with those of ATP-competitive inhibitors that blocked the phosphorylation of mTORC1 substrates regardless of their affinity for the

kinase.[39] Accordingly, these results strongly suggested that DHM25 was a competitive mTOR inhibitor (Fig. 3B-C).

The (*S*)-DHM25 enantiomer kills cancer cells and inhibits mTOR more efficiently than (*R*)-DHM25.

More than half of drugs are chiral compounds, and 90% of these molecules are marketed as racemic mixtures. Because enantiomers do not show the same spatial arrangement, their biological, pharmacodynamic, and pharmacokinetic properties can differ. In addition, the US Food and Drug Administration (FDA) recommends that the activity of each enantiomer be evaluated for racemic drugs and that chiral drugs be developed as single enantiomers.[40] DHM25 is a chiral molecule due to its stereogenic carbon atom, C2 (Fig. 4A). To evaluate the therapeutic activity of both DHM25 stereoisomers, the (*R*)- and (*S*)- enantiomers were separated by HPLC, and the absolute configuration of their chiral centers was determined using circular dichroism (Fig. S4). Next, the biological effects of (*R*)- and (*S*)-DHM25 were evaluated on Jurkat and CEM leukemic T cells (Fig. 4B-C). Although the difference was not large, (*S*)-DHM25 killed leukemic T cells more efficiently than its isomer (Fig. 4B), and this increased cytotoxic effect correlated with a greater inhibition of mTOR activity (Fig. 4C). In summary, (*S*)-DHM25 showed a slightly better mTOR inhibitory effect than its enantiomer, but this difference was not substantial enough to merit separating the two enantiomers in subsequent experiments.

Molecular simulations were next undertaken to understand why (*S*)-DHM25 targeted mTOR while (*S*)-DHM9 did not (Fig. S5A). Structural models of DHM9 and DHM25 within the ATP pocket of mTOR provided the first basis for understanding the binding modes and structure-activity relationships (SAR) of these compounds. First, the presence of the additional bromine in DHM25 compared to DHM9 influenced its position inside the ATP

pocket of mTOR (Fig. S5A-B). While DHM9 seemed to be preferentially positioned in the adenine pocket, DHM25 overlapped both the adenine pocket and the affinity pocket, notably through interactions with hinge residues Ile2237, Trp2239, and Val2240 at one side and with P-loop residues Ile2163, Ser2165, and Gln2167 at the other side, which are all also ATP-contact amino acids (Fig. S5C). Because interactions between chromene derivatives and the mTOR catalytic pocket were mainly driven through hydrophobic contacts, the dynamics of the ligand-free diffusion into the ATP pocket were further investigated. A contact frequency analysis over simulated trajectories confirmed that DHM25 interacted with more key amino acid residues (about 80% of ATP experimental contacts) in comparison to DHM9 (only 60% of ATP contacts, Fig. S5C). Models highlighted that unlike DHM9, DHM25 interacted inside the ATP-binding pocket of mTOR with amino acid residues of the P-loop (Fig. 4D). It is noteworthy that despite the fact that these P-loop basic amino acids showed a relatively high level of conservation among the PI3KK family members (Fig. S6A), this stretch of positively charged amino acids was lost in the sequences of PI3K family members (Fig. S6B), potentially explaining why DHM25 exhibited a selectivity for mTOR.

DHM25 is an irreversible mTOR inhibitor.

Computer modeling was next used to design and synthesize two molecular tools in order to confirm that this novel drug interacted with mTOR. Based on the most stable position of both the (*R*) and (*S*) enantiomers of DHM25 inside the catalytic pocket of mTOR, DHM25 was conjugated with a probe (biotin or FITC, Scheme 2) at the C6 position (solvent front position, Fig. 5A). Strikingly, confocal microscopy revealed that breast cancer cells treated with DHM25-FITC exhibited a dot-like distribution pattern (Fig. 5B) that co-localized with mTOR labeled with an anti-mTOR mAb (yellow color in the merge panel, Pearson's coefficient = 0.899, Fig. 5B). In agreement with modeling analyses, conjugation of biotin to C6 of DHM25

did not alter its inhibitory effect on mTORC2 activity (Fig. 5C). More importantly, a pull-down assay using streptavidin beads confirmed that DHM25-biotin interacted with mTOR (Fig. 5D). In addition, the affinity of DHM25-biotin for mTOR was stronger than that of DHM9-biotin (Fig. 5E). Overall, these findings confirmed that DHM25 was an mTOR inhibitor.

Modeling analysis also suggested that the electrophilic C4 in DHM25 was close enough to the lysine at position 2187 (K2187; see Fig. 6A and S5) in the mTOR catalytic domain to undergo a covalent link through a Michael reaction (Fig. 6A). In agreement with this observation, the DHM25-biotin/mTOR interaction was not lost after cell lysis under denaturing/reducing/boiling conditions (Fig. 5D-E). In addition, whereas extensive washing after 2 hours of incubation with the reversible mTOR inhibitor AZD8055 led to a rapid restoration of Akt phosphorylation at serine 473, identical treatment with DHM25 did not, suggesting an irreversible association with the kinase (Fig. 6B). To confirm this possibility, two types of DHM25 modifications were performed. First, a DHM25 derivative was synthesized in which the C3-C4 double bond was reduced (Scheme 3 and Fig. 6C). Conversion of the C3-C4 double bond into a single C-C bond removes the electrophilic property of the carbon at position C4 and its ability to form a covalent bond with the nitrogen atom at K2187. Of note, DHM25-H2 showed a dramatic reduction in cytotoxicity toward leukemic (Jurkat and CEM) and breast cancer cells (Fig. 6D) as compared to DHM25, and also lost its ability to inhibit phosphorylation of mTORC1 (4E-BP1) and mTORC2 (Akt-S473) substrates (Fig. 6E). Next, NO_2, a strong electron-withdrawing group (EWG) in DHM25 was replaced by various chemical groups to reduce the capacity of C4 to act as an electron acceptor. To this end, four chromologs were prepared in which the NO_2 group was replaced by aldehyde (LR20), amide (LR28), ester (LR29), or carboxylic acid (LR24) functional groups showing an electrophilic strength gradient (Scheme 4). Except for LR29,

the lower the withdrawing capacity of the substituted group, the weaker the cytotoxic activity of the resulting compound (Fig. 6F). In agreement with this observation, the decreased cytotoxic activity of LR20 (replacement of NO_2 by an aldehyde) and LR28 (replacement of NO_2 by an amide functional group) toward CEM and Jurkat cells (Fig. 6F) was associated with their inability to inhibit Akt phosphorylation at Ser473 (Fig. 6G). These chemical modifications of DHM25 provided some insights into how carbon 4 could serve as a Michael acceptor to covalently bind lysine at position 2187 inside the ATP pocket of mTOR. Overall, these findings revealed that DHM25 could act as a covalent inhibitor of mTOR.

DHM25 inhibits CD95-mediated cell migration and prevents *in vivo* tumor progression of TNBC cells.

CD95L (also known as FasL) belongs to the TNF (tumor necrosis factor) family and is the ligand for the "death receptor" CD95 (Fas/APO1). This transmembrane receptor can be cleaved by metalloproteases[41] to produce a soluble ligand. This naturally processed CD95L (cl-CD95L) is increased in patients affected by TNBC and enhances the risk of metastatic dissemination in these patients.[42] Unlike membrane-bound CD95L, cl-CD95L fails to induce apoptosis and instead promotes the formation of an atypical receptosome that we designated the motility-inducing signaling complex (MISC).[43] MISC formation leads to the induction of the pro-oncogenic PI3K/mTOR signaling pathway.[43, 44] The ability of DHM25 to prevent this CD95-mediated cell migration was assessed in TNBC cells. To address this question, the highest dose of DHM25 that did not cause cell death in two TNBC cell lines (BT549 and MDA-MB-231) was determined (Fig. 7A). In Boyden chamber assays, although 1 μM DHM25 did not exhibit any cytotoxicity (Fig. 7A), it inhibited the CD95-mediated PI3K/mTOR activation (data not shown) and abrogated CD95-mediated cell migration in TNBC cells (Fig. 7B).

Finally, the *in vivo* therapeutic activity of DHM25 against TNBCs was assessed. In immunodeficient NOD/SCID/γc (NSG) mice, the maximum intravenous tolerated dose of DHM25 was 10 mg/kg (Fig. S7A-B). Human MDA-MB-231 TNBC cells were orthotopically (mammary fat pad) transplanted in NSG mice, and when tumors were palpable, mice received repeated intravenous injections of DHM25 (10 mg/kg) or vehicle. DHM25 treatment significantly and markedly reduced primary tumor growth (primary site, Fig. 7C) and prevented distant metastasis to lungs (classical secondary tumor site) (Fig. 7C). In conclusion, we generated an irreversible and competitive mTOR inhibitor that exhibited *in vivo* anti-tumor activity against TNBC cells.

DISCUSSION & CONCLUSIONS

Using different tumor cell lines characterized for their high or low reliance on the PI3K/mTOR signaling pathway for survival, classical biochemical analysis (Akt phosphorylation), large-scale kinase profiling, and several rounds of chemical synthesis, we developed a novel irreversible inhibitor of mTOR showing *in vitro* and *in vivo* cytotoxic activity against breast cancer cells.

Inactivation of the DHM25 electrophilic warhead reduces or abrogates its ability to inhibit mTOR activity, indicating that its mechanism of inhibition occurs mainly through its capacity to covalently interact with a nucleophilic amino acid inside the ATP pocket. In agreement with this, DHM25 analogs with an inactivated warhead (DHM25-H2) or a reduced electrophilic C4, which were generated by replacing the strong EWG NO_2, indicate that the carbon at position 4 undergoes a nucleophilic attack, probably by K2187 in the mTOR catalytic pocket. Also, washout experiments show that whereas transient incubation with the reversible mTOR inhibitor AZD8055 allows for the rapid recovery of mTOR activity, similar treatment with DHM25 does not. This latter experiment highlights one of the advantages expected *in vivo* with mTOR covalent inhibitors, namely, prolonged action even when the drug has been systemically eliminated. Indeed, the overall pharmacological effect *in vivo* will be largely dependent on the *de novo* protein synthesis rate (the half-life of mTOR is approximately 18 hours[45]). Of note, PI3K lipid kinases and PI3KK members such as mTOR share motifs in their catalytic domain,[46] and K2187 in mTOR is a highly conserved motif among all PI3K members (Fig. S6B), which suggested that DHM25 might also be an inhibitor of PI3Ks. Nonetheless, our study ruled out this possibility. Also, although DHM25 and DHM9 differ only by one bromine, they inhibit a completely different set of kinases (Fig. 3A), illustrating that although the covalent bond in the ATP pocket of mTOR is instrumental in the ability of DHM25 to inhibit mTOR, the electrophilic warheads of DHM25, DHM9, and

S14161 must be properly oriented for a prolonged time within the targeted protein to efficiently undergo the appropriate nucleophilic Michael addition. Our hypothesis is that by interacting with mTOR P-loop residues, DHM25 has better positioning and stronger stability than DHM9 inside the ATP pocket, favoring its nucleophilic attack by K2187.

It is noteworthy that some covalent drugs have been evaluated in clinical trials and been approved by the US FDA.[47, 48] Although the risks of covalent inhibitors are known (compounds with reactive functionality and potentially increased off-target interactions), the sustained duration of inhibition of covalent inhibitors yields a number of potential advantages, including improved inhibitory activity, as competition with endogenous substrates is reduced. Another advantage is the dissociation of pharmacokinetics from pharmacodynamics (PD), as PD relies on protein resynthesis. This means that covalent drugs can be clinically useful even if their half-lives are short, as only a short exposure would be required for the drug to reach its molecular target and inhibit it for a prolonged period of time.

There is no approved targeted therapy for TNBC, and TNBC patients are treated with traditional chemotherapy alone. In the first 3 years after diagnosis, TNBC patients account for a disproportionate number of early deaths not only due to its aggressive nature but also because of the lack of targeted therapeutic treatment options.[49] Therefore, there is a crucial need for targeted therapy for this pathology. We recently demonstrated that after cleavage by metalloprotease, soluble CD95L promotes metastatic dissemination of TNBC cells by activating an atypical PI3K/mTOR signaling pathway.[50] The current study demonstrates that DHM25 is not only able to kill TNBC cells *in vitro* and *in vivo*, but it can also block cell migration of TNBC cells exposed to soluble CD95L at non-cytotoxic (low) concentrations. These data clearly suggest that DHM25, alone or in combination with classical chemotherapy, may be an attractive therapeutic option not only as a primary therapy for TNBC patients but also to reduce/prevent the risk of metastatic occurrence in TNBC patients with high

concentrations of serum CD95L.

Among 52 ongoing clinical trials exploring the therapeutic effect of mTOR inhibitors on breast cancer patients, only four are being conducted in metastatic TNBCs using derivatives of the mTORC1 inhibitor rapamycin (*e.g.*, temsirolimus or everolimus) or an imidazoquinoline derivative called BEZ235 (ClinicalTrials.gov). Nonetheless, preliminary results from these studies confirmed those obtained with temsirolimus and everolimus in individuals with metastatic breast cancer.[51, 52] Indeed, rapalogs are primarily cytostatic, not cytotoxic, and clinical efficacy largely reflects disease stabilization rather than regression.[19] One reason for the compromised clinical benefit of rapalogs is that by only targeting mTORC1, they release the negative feedback circuits of this molecular complex, driving mitogenic signaling by activating the upstream PI3K pathway.[19] Indeed, mTORC1-driven activation of p70S6K induces insulin receptor substrate degradation, which in turn reduces PI3K activation.[53] Also, p70S6K phosphorylates Rictor to inhibit mTORC2 activity[54, 55] and thereby reduces mTORC2-mediated Akt activation. Consequently, everolimus-mediated mTORC1 inhibition leads to Akt activation in tumor biopsies of colon cancers.[12] Overall, this evidence suggests that competitive inhibitors of mTOR that target both mTORC1 and mTORC2 may represent attractive opportunities to treat PI3K-addicted malignant tumors such as TNBC.

EXPERIMENTAL SECTION

Chemistry

General information. All reagents and solvents were used as purchased from commercial suppliers or were purified/dried according to Armarego W. L. F. and Chai C. L. L. (Purification of Laboratory Chemicals, 6th edition, Elsevier). ^{1}H and ^{13}C-NMR spectra were recorded on a Bruker Avance 300 or 500 instrument using TMS and $CDCl_3$ respectively as internal standard. Chemical shifts (δ values) are given in parts per million (ppm), coupling constants (J values) are given in Hertz (Hz), and multiplicity of signals is reported as usual. HRMS analyzes were obtained using a Waters Q-TOF 2 or a Bruker MicrO-TOF Q II instrument for ESI. Optical rotations were recorded on a Perkin Elmer Model 341 polarimeter. The purity of final tested compounds was typically determined to be $\geqslant$95% by HPLC, conducted on a Shimadzu Prominence system using a Grace Prevail C18 column and diode array detector. Chiral HPLC was performed using a Daicel Chiralpak IA column. Elementary analysis of the injected DHM25 was performed on a Thermo-fisher ICAP 6500 Duo instrument. Melting points were obtained on a hot bench. VCD spectra were measured on a Bruker Optics Vertex 70 spectrometer and ECD spectra using a Jasco J815 spectrometer. TLC analyzes were performed using precoated Merck TLC Silica Gel 60 F_{254} plates. Purifications by column chromatography on silica gel were performed using Grace Davisil Silica Gel 60 (70-200 mesh and 40-60 mesh) and purifications by preparative thin layer chromatography on silica gel using Merck Silica Gel 60 PF_{254}. Petroleum ether (PE) used for purifications was the low boiling point fraction (40-60 °C).

General procedure for the synthesis of chromenes. The mixture of Michael acceptor derivative (1.0 mmol), salicylaldehyde compound (1.0 mmol, 1.0 eq.) and organocatalyst (0.2 mmol, 0.2 eq.) in 1.5 mL of dry toluene was heated at 80-100 °C for 48-72 h under inert

atmosphere (conversion followed by TLC). After cooling to room temperature, the mixture was charged directly on the silica gel column for purification.

*Description of the title compounds: 6,8-Dibromo-2-(4-bromophenyl)-3-nitro-2H-chromene (**DHM25**)*

Mp = 150-152 °C. ^{1}H NMR (300 MHz, $CDCl_3$) δ 6.67 (s, 1H), 7.24 (d, J = 8.5, 2H), 7.40 (d, J = 2.2, 1H), 7.48 (d, J =8.5, 2H), 7.67 (d, J = 2.2, 1H), 7.95 (s, 1H). ^{13}C NMR (75 MHz, $CDCl_3$) δ 74.1, 112.6, 115.0, 120.7, 124.3, 127.7, 128.6, 131.7, 132.3, 134.8, 139.3, 142.4, 149.4. HRMS $[M+H]^+$ calculated for $C_{15}H_9NO_3Br_3$ 487.8132, found 487.8133. Anal. calculated for $C_{15}H_9NO_3Br_3$: C, 36.77; H, 1.65, N, 2.86. found: C, 36.29, H, 1.56, N, 2.73. (*S*)-DHM25: $[\alpha]_D$ = +154.6 (c = 1, $CHCl_3$); (*R*)-DHM25: $[\alpha]_D$ = -157.7 (c = 1, $CHCl_3$).

Cell Lines

All cells were obtained from ATCC (LGC Standards, Molsheim, France). The leukemic T-cell lines CEM, Jurkat and H9 were cultured in RPMI1640 supplemented with 8% heat-inactivated FCS and 2 mM L-glutamine in a 5% CO_2 incubator at 37 °C. All breast tumor cells were cultured in DMEM supplemented with 8% heat-inactivated FCS and 2 mM L-glutamine in a 5% CO_2 incubator at 37 °C.

Antibodies, plasmids and other reagents.

LY294002 and Wortmannin were obtained from Calbiochem (Merck Chemicals Ltd., Nottingham, UK). AZD8055 was from Selleckchem (Munich, Germany). The chromene and chromene derivatives are solubilized in DMSO (20 mM). Anti-β-actin was purchased from Sigma (L'Isle-d'Abeau-Chesnes, France). Anti-Akt, anti-Akt-P^{S473}, anti-4E-BP1, anti-4E-BP1-$P^{Thr37/46}$, anti-S6, anti-S6K-$P^{Ser240/244}$, anti-PTEN and anti-mTOR were from Cell Signaling Technology (Boston, MA, USA).

Molecular Modeling

mTOR structural model was based on the X-ray experimental structure provided by the Protein Data Bank (PDB ID: 4JSN[56]) and completed for the missing residues (1814-1867 and 2436-2492) by homology modelling tools distributed by Yasara.[57] DHM compounds were parametrized for the Yamber3 force field following the automated AutoSMILE procedure, consisting in AM1 quantum calculation and RESP charge fitting protocol. Initial positions of DHM compounds have been set by analogy to the quercetin placement in the PI3K catalytic site (PDB ID: 1E8W[58]) because of the similarity in the chemical scaffold of ligands and catalytic site of proteins. Each molecular complex was simulated in a neutralized explicit water solvent box, under periodic boundary conditions and at a constant temperature of 298 K. Molecular dynamics (MD) trajectories of 62 nanoseconds were collected at 2 picoseconds intervals for both molecular systems. Production period used for analysis was set after the MD simulation reach an equilibrated state (stable root mean square deviation). Clustering analysis upon trajectories were performed using the Jarvis-Patrick method implemented in Gromacs tools.[59]

Pull down assay

CEM cells (10^7) were pre-incubated with indicated concentrations of DHM25, its biotin-conjugated counterpart or DHM9-biotin for 2h at 37 °C. Then cells were lysed in a denaturating buffer (50mM Tris pH 7.4, 2 mM EDTA, 150 mM NaCl, 50 mM NaF, 0.5% Na-deoxycholate monohydrate, 1% Triton X-100, 0.1% SDS) complemented with protease and phosphatase inhibitors (Sigma) and biotin-conjugated DHM9 or DHM25 was immunoprecipitated using streptavidin magnetic beads (Ademtech, Pessac, France) for 1 h at 4 °C. After extensive washing, the immune complex was resuspended in a denaturing and reducing Laemmli Sample Buffer (60 mM Tris-Cl pH 6.8, 2% SDS, 10% glycerol, 5% β-

mercaptoethanol, 0.01% bromophenol blue), resolved by SDS/PAGE and revealed by Western blot.

Circular dichroism

Both enantiomers were obtained by resolution of racemic DHM25 using chiral HPLC (Chiralpak IA column, MeOH as eluent, 1.0 mL/min: $RT_{DHM25\text{-}E1}$ = 8.13 min, $RT_{DHM25\text{-}E2}$ = 10.48 min). The absolute configuration of each DHM25 enantiomer was determined by vibrational and electronic circular dichroism (VCD and ECD) by comparison of experimental to predicted spectra. VCD spectra were recorded on a Bruker Vertex70 spectrometer (with a PMA50 module) and theoretical simulated VCD obtained by the SMD/B3PLYP/6-311+G(d,p)/Lanl2dz method. ECD analyses were performed on a Jasco J815 spectrometer and theoretical simulated ECD obtained by the SMD/TD-CAMB3LYP/6-31++G(d,p)/Lanl2dz method. Thus DHM25-E1 was identified as the (*S*) enantiomer and DHM25-E2 as the (*R*) one.

Reversibility experiments

CEM cells (2×10^6) were treated in the presence or absence of DHM25 (5 μM) or AZD8055 (5 μM) for 2 h at 37 °C. Next, cells were extensively washed to eliminate the excess of inhibitor and cells were resuspended in fresh medium. Restoration of mTOR activity was evaluated by monitoring at different times the phosphorylation level of Akt at Serine 473.

Detergent Lysis experiments and Western Blot Analysis

Cell lyses and western blot analyses were performed exactly as previously described.[33]

Measure of cell death

Cell death was assessed using either the viability MTT assay.[60]

Immunoblot analysis.

Cells were lysed for 30 min at 4 °C in lysis buffer [25 mM HEPES (pH 7.4), 1% v/v Triton X-100, 150 mM NaCl, and 2 mM EGTA supplemented with a mix of protease inhibitors (Sigma)]. Protein concentration was determined by the bicinchoninic acid method (Pierce, Rockford, IL, USA). Proteins were separated by SDS-PAGE and transferred to a nitrocellulose membrane. The membrane was blocked for 30 min with TBST (50 mM Tris, 160 mM NaCl, 0.05% v/v Tween 20, pH 7.8) containing 5% w/v dried skimmed milk and then incubated overnight with primary antibody at 4°C in TBSTM. The membrane was washed (TBST) and secondary HRP-labeled antibody (SouthernBiotech, US) was added for 45 min. The proteins were visualized with the enhanced chemiluminescence substrate kit (Pierce).

Kinase profiler screening

To evaluate the kinases targeted by DHM25 and DHM9, Kinase Profiler Service (Millipore) was used with 243 available kinases. The screening was performed with 1 μM of compound and 10 μM ATP and kinase substrates according to Millipore's protocol.

Immunofluorescence imaging.

MDA-MB-231 cells were incubated for 3 hours at 37 °C with DHM25-FITC (10 μM) or FITC alone. Cells were then washed twice in PBS and fixed for 15 min in PBS containing 4% w/v paraformaldehyde. The aldehyde groups were quenched for 10 min in PBS supplemented with 5% FCS. mTOR was visualized by using 5 μg/ml of goat anti-mTOR mAb (N19, Santa-Cruz, CA, USA) incubated for 20 min at 4 °C, washed and incubated for another 20 min at 4

°C with anti-goat IgG (H+L) coupled with Alexa Fluor 594-conjugated antibody (Life Technologies, CA, USA). Finally, cells were washed twice with PBS, dried, and mounted with 20 µl of mounting medium (Sigma, MO, USA). Images were acquired using a laser scanning confocal system (TCS SP8 model mounted on a DMI 6000 CS inverted microscope, Leica, Heidelberg, Germany). Images were taken using a 40x oil-immersion objective (1.3, N.A.) and analysed using the ImageJ software (NIH, Bethesda, Maryland, USA).

In vitro motility assays.

After membrane hydration of Boyden chambers (Millipore, Molsheim, France) containing 8 µm pore membranes, 10^5 cells were added to the top chamber. The bottom chamber was filled with low serum (1%)-containing medium in the presence or absence of cl-CD95L (100 ng/ml). Breast cancer cells were incubated for 24 h. To quantify invasion, cells were fixed with methanol and stained with Giemsa. Stained cells were then removed from the top-side of the membrane using a cotton-tipped swab and five representative pictures for each insert were taken of the invading cells from the reverse side. For each experiment, invading cells were lysed and absorbance at 560 nm was measured.

Mouse experiments.

NOD/SCID/γc null mice (NSG) were obtained from Dr C. Rivers (UK). All experiments were performed in agreement with the French Guidelines for animal handling and approved by local ethics committee. Luciferase-expressing MDA-MB-231 cells (5×10^5 cells in 50 μL PBS/Matrigel) were transplanted into mammary fat pads of mice (7 *weeks old female)*. Once tumors were palpable, intraperitoneal injection of DHM25 resuspended in PBS/Tween-80/DMSO (8/1/1) or control medium was performed repeatedly 5 days a week until day 46. Bioluminescence analysis was performed using PhotonIMAGER (Biospace Lab) following of

endotoxin-free luciferin (30 mg/kg). Tumor volume was calculated using the formula V = 0.52 (L×W2). After completion of the analysis, autopsy of mice was done, and organ luminescence was assessed.

SUPPORTING INFORMATION AVAILABLE: Full experimental details are given in the supporting information document. This material is available free of charge via the Internet at http://pubs.acs.org.

[*]**CORRESPONDING AUTHOR INFORMATION:** Dr. Patrick Legembre, Phone: (+33)-2-2323-7241, Fax: (+33)-2-9925-3164, E-mail: patrick.legembre@inserm.fr. Prof. Pierre van de Weghe, Phone: (+33)-2-2323-3803, Fax: (+33)-2-2323-4425, E-mail: pierre.van-de-weghe@univ-rennes1.fr.

[8]**AUTHOR CONTRIBUTIONS:** Authors share corresponding authorship.

ACKNOWLEDGEMENTS:

This work was supported by grants from Ligue Contre le Cancer (Comités d'Ille-et-Vilaine, du Morbihan, des Côtes d'Armor, du Finistère et du Maine et Loire), INCa PLBIO, Ouest Valorisation and Fondation ARC. A.F. is supported by INCa. The authors also thank members of the TrGET and CRCM animal facilities for their technical assistance. TrGET is supported by Institut Paoli-Calmettes (IPC) and Canceropôle PACA. The authors thank the PRISM platform (Université Rennes-1) for NMR experiments.

ABBREVIATIONS USED:

mTOR: mammalian target of rapamycin; mTORC1 and C2: mammalian target of rapamycin complex 1 and 2; PI3K: Phosphatidylinositol-4,5-bisphosphate 3-kinase; PI3KK: phosphatidylinositol 3-OH-kinase-related kinase; TNBC: triple-negative breast cancers.

REFERENCES

1. Myers, M. P.; Pass, I.; Batty, I. H.; Van der Kaay, J.; Stolarov, J. P.; Hemmings, B. A.; Wigler, M. H.; Downes, C. P.; Tonks, N. K. The lipid phosphatase activity of PTEN is critical for its tumor supressor function. *Proc Natl Acad Sci U S A.* **1998,** 95, 13513-13518.

2. Stambolic, V.; Suzuki, A.; de la Pompa, J. L.; Brothers, G. M.; Mirtsos, C.; Sasaki, T.; Ruland, J.; Penninger, J. M.; Siderovski, D. P.; Mak, T. W. Negative regulation of PKB/Akt-dependent cell survival by the tumor suppressor PTEN. *Cell.* **1998,** 95, 29-39.

3. Gewinner, C.; Wang, Z. C.; Richardson, A.; Teruya-Feldstein, J.; Etemadmoghadam, D.; Bowtell, D.; Barretina, J.; Lin, W. M.; Rameh, L.; Salmena, L.; Pandolfi, P. P.; Cantley, L. C. Evidence that inositol polyphosphate 4-phosphatase type II is a tumor suppressor that inhibits PI3K signaling. *Cancer Cell.* **2009,** 16, 115-125.

4. Alessi, D. R.; James, S. R.; Downes, C. P.; Holmes, A. B.; Gaffney, P. R.; Reese, C. B.; Cohen, P. Characterization of a 3-phosphoinositide-dependent protein kinase which phosphorylates and activates protein kinase Balpha. *Curr Biol.* **1997,** 7, 261-269.

5. Guertin, D. A.; Stevens, D. M.; Thoreen, C. C.; Burds, A. A.; Kalaany, N. Y.; Moffat, J.; Brown, M.; Fitzgerald, K. J.; Sabatini, D. M. Ablation in mice of the mTORC components raptor, rictor, or mLST8 reveals that mTORC2 is required for signaling to Akt-FOXO and PKCalpha, but not S6K1. *Dev Cell.* **2006,** 11, 859-871.

6. Gao, X.; Zhang, Y.; Arrazola, P.; Hino, O.; Kobayashi, T.; Yeung, R. S.; Ru, B.; Pan, D. Tsc tumour suppressor proteins antagonize amino-acid-TOR signalling. *Nat Cell Biol.* **2002,** 4, 699-704.

7. Inoki, K.; Li, Y.; Zhu, T.; Wu, J.; Guan, K. L. TSC2 is phosphorylated and inhibited by Akt and suppresses mTOR signalling. *Nat Cell Biol.* **2002,** 4, 648-657.

8. Tee, A. R.; Fingar, D. C.; Manning, B. D.; Kwiatkowski, D. J.; Cantley, L. C.; Blenis, J. Tuberous sclerosis complex-1 and -2 gene products function together to inhibit mammalian

target of rapamycin (mTOR)-mediated downstream signaling. *Proc Natl Acad Sci U S A.* **2002,** 99, 13571-13576.

9. Inoki, K.; Li, Y.; Xu, T.; Guan, K. L. Rheb GTPase is a direct target of TSC2 GAP activity and regulates mTOR signaling. *Genes Dev.* **2003,** 17, 1829-1834.

10. Sarbassov, D. D.; Guertin, D. A.; Ali, S. M.; Sabatini, D. M. Phosphorylation and regulation of Akt/PKB by the rictor-mTOR complex. *Science.* **2005,** 307, 1098-1101.

11. Manning, B. D.; Logsdon, M. N.; Lipovsky, A. I.; Abbott, D.; Kwiatkowski, D. J.; Cantley, L. C. Feedback inhibition of Akt signaling limits the growth of tumors lacking Tsc2. *Genes Dev.* **2005,** 19, 1773-1778.

12. O'Reilly, K. E.; Rojo, F.; She, Q. B.; Solit, D.; Mills, G. B.; Smith, D.; Lane, H.; Hofmann, F.; Hicklin, D. J.; Ludwig, D. L.; Baselga, J.; Rosen, N. mTOR inhibition induces upstream receptor tyrosine kinase signaling and activates Akt. *Cancer Res.* **2006,** 66, 1500-1508.

13. Vezina, C.; Kudelski, A.; Sehgal, S. N. Rapamycin (AY-22,989), a new antifungal antibiotic. I. Taxonomy of the producing streptomycete and isolation of the active principle. *J Antibiot (Tokyo).* **1975,** 28, 721-726.

14. Brown, E. J.; Albers, M. W.; Shin, T. B.; Ichikawa, K.; Keith, C. T.; Lane, W. S.; Schreiber, S. L. A mammalian protein targeted by G1-arresting rapamycin-receptor complex. *Nature.* **1994,** 369, 756-758.

15. Sabatini, D. M.; Erdjument-Bromage, H.; Lui, M.; Tempst, P.; Snyder, S. H. RAFT1: a mammalian protein that binds to FKBP12 in a rapamycin-dependent fashion and is homologous to yeast TORs. *Cell.* **1994,** 78, 35-43.

16. Chiu, M. I.; Katz, H.; Berlin, V. RAPT1, a mammalian homolog of yeast Tor, interacts with the FKBP12/rapamycin complex. *Proc Natl Acad Sci U S A.* **1994,** 91, 12574-12578.

17. Populo, H.; Lopes, J. M.; Soares, P. The mTOR Signalling Pathway in Human Cancer. *Int J Mol Sci.* **2012,** 13, 1886-1918.

18. Crino, P. B.; Nathanson, K. L.; Henske, E. P. The tuberous sclerosis complex. *N Engl J Med.* **2006,** 355, 1345-1356.

19. Wander, S. A.; Hennessy, B. T.; Slingerland, J. M. Next-generation mTOR inhibitors in clinical oncology: how pathway complexity informs therapeutic strategy. *J Clin Invest.* **2011,** 121, 1231-1241.

20. Grunt, T. W.; Mariani, G. L. Novel approaches for molecular targeted therapy of breast cancer: interfering with PI3K/AKT/mTOR signaling. *Curr Cancer Drug Targets.* **2013,** 13, 188-204.

21. Ferlay, J.; Parkin, D. M.; Steliarova-Foucher, E. Estimates of cancer incidence and mortality in Europe in 2008. *Eur J Cancer.* **2010,** 46, 765-781.

22. Sotiriou, C.; Pusztai, L. Gene-expression signatures in breast cancer. *N Engl J Med.* **2009,** 360, 790-800.

23. Perou, C. M.; Sorlie, T.; Eisen, M. B.; van de Rijn, M.; Jeffrey, S. S.; Rees, C. A.; Pollack, J. R.; Ross, D. T.; Johnsen, H.; Akslen, L. A.; Fluge, O.; Pergamenschikov, A.; Williams, C.; Zhu, S. X.; Lonning, P. E.; Borresen-Dale, A. L.; Brown, P. O.; Botstein, D. Molecular portraits of human breast tumours. *Nature.* **2000,** 406, 747-752.

24. Paik, S.; Shak, S.; Tang, G.; Kim, C.; Baker, J.; Cronin, M.; Baehner, F. L.; Walker, M. G.; Watson, D.; Park, T.; Hiller, W.; Fisher, E. R.; Wickerham, D. L.; Bryant, J.; Wolmark, N. A multigene assay to predict recurrence of tamoxifen-treated, node-negative breast cancer. *N Engl J Med.* **2004,** 351, 2817-2826.

25. Chin, K.; DeVries, S.; Fridlyand, J.; Spellman, P. T.; Roydasgupta, R.; Kuo, W. L.; Lapuk, A.; Neve, R. M.; Qian, Z.; Ryder, T.; Chen, F.; Feiler, H.; Tokuyasu, T.; Kingsley, C.; Dairkee, S.; Meng, Z.; Chew, K.; Pinkel, D.; Jain, A.; Ljung, B. M.; Esserman, L.; Albertson,

D. G.; Waldman, F. M.; Gray, J. W. Genomic and transcriptional aberrations linked to breast cancer pathophysiologies. *Cancer Cell.* **2006,** 10, 529-541.

26. Foulkes, W. D.; Stefansson, I. M.; Chappuis, P. O.; Begin, L. R.; Goffin, J. R.; Wong, N.; Trudel, M.; Akslen, L. A. Germline BRCA1 mutations and a basal epithelial phenotype in breast cancer. *J Natl Cancer Inst.* **2003,** 95, 1482-1485.

27. Comprehensive molecular portraits of human breast tumours. *Nature.* **2012,** 490, 61-70.

28. Miller, T. W.; Rexer, B. N.; Garrett, J. T.; Arteaga, C. L. Mutations in the phosphatidylinositol 3-kinase pathway: role in tumor progression and therapeutic implications in breast cancer. *Breast Cancer Res.* **2011,** 13, 224.

29. Mao, X.; Cao, B.; Wood, T. E.; Hurren, R.; Tong, J.; Wang, X.; Wang, W.; Li, J.; Jin, Y.; Sun, W.; Spagnuolo, P. A.; MacLean, N.; Moran, M. F.; Datti, A.; Wrana, J.; Batey, R. A.; Schimmer, A. D. A small-molecule inhibitor of D-cyclin transactivation displays preclinical efficacy in myeloma and leukemia via phosphoinositide 3-kinase pathway. *Blood.* **2011,** 117, 1986-1997.

30. Dondoni, A.; Massi, A. Asymmetric organocatalysis: from infancy to adolescence. *Angew Chem Int Ed Engl.* **2008,** 47, 4638-4660.

31. Seayad, J.; List, B. Asymmetric organocatalysis. *Org Biomol Chem.* **2005,** 3, 719-724.

32. Dalko, P. I.; Moisan, L. In the golden age of organocatalysis. *Angew Chem Int Ed Engl.* **2004,** 43, 5138-5175.

33. Beneteau, M.; Pizon, M.; Chaigne-Delalande, B.; Daburon, S.; Moreau, P.; De Giorgi, F.; Ichas, F.; Rebillard, A.; Dimanche-Boitrel, M. T.; Taupin, J. L.; Moreau, J. F.; Legembre, P. Localization of Fas/CD95 into the lipid rafts on down-modulation of the phosphatidylinositol 3-kinase signaling pathway. *Mol Cancer Res.* **2008,** 6, 604-613.

34. Pizon, M.; Rampanarivo, H.; Tauzin, S.; Chaigne-Delalande, B.; Daburon, S.; Castroviejo, M.; Moreau, P.; Moreau, J. F.; Legembre, P. Actin-independent exclusion of CD95 by PI3K/AKT signalling: implications for apoptosis. *Eur J Immunol.* **2011,** 41, 2368-2378.

35. Hresko, R. C.; Mueckler, M. mTOR.RICTOR is the Ser473 kinase for Akt/protein kinase B in 3T3-L1 adipocytes. *J Biol Chem.* **2005,** 280, 40406-40416.

36. Laplante, M.; Sabatini, D. M. mTOR signaling at a glance. *J Cell Sci.* **2009,** 122, 3589-3594.

37. Jacinto, E.; Loewith, R.; Schmidt, A.; Lin, S.; Ruegg, M. A.; Hall, A.; Hall, M. N. Mammalian TOR complex 2 controls the actin cytoskeleton and is rapamycin insensitive. *Nat Cell Biol.* **2004,** 6, 1122-1128.

38. Sarbassov, D. D.; Ali, S. M.; Kim, D. H.; Guertin, D. A.; Latek, R. R.; Erdjument-Bromage, H.; Tempst, P.; Sabatini, D. M. Rictor, a novel binding partner of mTOR, defines a rapamycin-insensitive and raptor-independent pathway that regulates the cytoskeleton. *Curr Biol.* **2004,** 14, 1296-1302.

39. Kang, S. A.; Pacold, M. E.; Cervantes, C. L.; Lim, D.; Lou, H. J.; Ottina, K.; Gray, N. S.; Turk, B. E.; Yaffe, M. B.; Sabatini, D. M. mTORC1 phosphorylation sites encode their sensitivity to starvation and rapamycin. *Science.* **2013,** 341, 1236566.

40. Ariens, E. J. Stereochemistry, a basis for sophisticated nonsense in pharmacokinetics and clinical pharmacology. *Eur J Clin Pharmacol.* **1984,** 26, 663-668.

41. Tauzin, S.; Debure, L.; Moreau, J. F.; Legembre, P. CD95-mediated cell signaling in cancer: mutations and post-translational modulations. *Cell Mol Life Sci.* **2012,** 69, 1261-1277.

42. Malleter, M.; Tauzin, S.; Bessede, A.; Castellano, R.; Goubard, A.; Godey, F.; Leveque, J.; Jezequel, P.; Campion, L.; Campone, M.; Ducret, T.; Macgrogan, G.; Debure, L.;

Collette, Y.; Vacher, P.; Legembre, P. CD95L cell surface cleavage triggers a prometastatic signaling pathway in triple-negative breast cancer. *Cancer Res.* **2013,** 73, 6711-6721.

43. Tauzin, S.; Chaigne-Delalande, B.; Selva, E.; Khadra, N.; Daburon, S.; Contin-Bordes, C.; Blanco, P.; Le Seyec, J.; Ducret, T.; Counillon, L.; Moreau, J. F.; Hofman, P.; Vacher, P.; Legembre, P. The naturally processed CD95L elicits a c-yes/calcium/PI3K-driven cell migration pathway. *PLoS Biol.* **2011,** 9, e1001090.

44. Kleber, S.; Sancho-Martinez, I.; Wiestler, B.; Beisel, A.; Gieffers, C.; Hill, O.; Thiemann, M.; Mueller, W.; Sykora, J.; Kuhn, A.; Schreglmann, N.; Letellier, E.; Zuliani, C.; Klussmann, S.; Teodorczyk, M.; Grone, H. J.; Ganten, T. M.; Sultmann, H.; Tuttenberg, J.; von Deimling, A.; Regnier-Vigouroux, A.; Herold-Mende, C.; Martin-Villalba, A. Yes and PI3K bind CD95 to signal invasion of glioblastoma. *Cancer Cell.* **2008,** 13, 235-248.

45. Takai, H.; Wang, R. C.; Takai, K. K.; Yang, H.; de Lange, T. Tel2 regulates the stability of PI3K-related protein kinases. *Cell.* **2007,** 131, 1248-1259.

46. Andrs, M.; Korabecny, J.; Jun, D.; Hodny, Z.; Bartek, J.; Kuca, K. Phosphatidylinositol 3-Kinase (PI3K) and phosphatidylinositol 3-kinase-related kinase (PIKK) inhibitors: importance of the morpholine ring. *J Med Chem.* **2015,** 58, 41-71.

47. Singh, J.; Petter, R. C.; Baillie, T. A.; Whitty, A. The resurgence of covalent drugs. *Nat Rev Drug Discov.* **2011,** 10, 307-317.

48. Sanderson, K. Irreversible kinase inhibitors gain traction. *Nat Rev Drug Discov.* **2013,** 12, 649-651.

49. Peto, R.; Davies, C.; Godwin, J.; Gray, R.; Pan, H. C.; Clarke, M.; Cutter, D.; Darby, S.; McGale, P.; Taylor, C.; Wang, Y. C.; Bergh, J.; Di Leo, A.; Albain, K.; Swain, S.; Piccart, M.; Pritchard, K. Comparisons between different polychemotherapy regimens for early breast cancer: meta-analyses of long-term outcome among 100,000 women in 123 randomised trials. *Lancet.* **2012,** 379, 432-444.

50. Malleter, M.; Tauzin, S.; Bessede, A.; Castellano, R.; Goubard, A.; Godey, F.; Leveque, J.; Jezequel, P.; Campion, L.; Campone, M.; Ducret, T.; Macgrogan, G.; Debure, L.; Collette, Y.; Vacher, P.; Legembre, P. CD95L cell surface cleavage triggers a pro-metastatic signaling pathway in triple negative breast cancer. *Cancer Res.* **2013**.

51. Chan, S.; Scheulen, M. E.; Johnston, S.; Mross, K.; Cardoso, F.; Dittrich, C.; Eiermann, W.; Hess, D.; Morant, R.; Semiglazov, V.; Borner, M.; Salzberg, M.; Ostapenko, V.; Illiger, H. J.; Behringer, D.; Bardy-Bouxin, N.; Boni, J.; Kong, S.; Cincotta, M.; Moore, L. Phase II study of temsirolimus (CCI-779), a novel inhibitor of mTOR, in heavily pretreated patients with locally advanced or metastatic breast cancer. *J Clin Oncol.* **2005,** 23, 5314-5322.

52. Ellard, S. L.; Clemons, M.; Gelmon, K. A.; Norris, B.; Kennecke, H.; Chia, S.; Pritchard, K.; Eisen, A.; Vandenberg, T.; Taylor, M.; Sauerbrei, E.; Mishaeli, M.; Huntsman, D.; Walsh, W.; Olivo, M.; McIntosh, L.; Seymour, L. Randomized phase II study comparing two schedules of everolimus in patients with recurrent/metastatic breast cancer: NCIC Clinical Trials Group IND.163. *J Clin Oncol.* **2009,** 27, 4536-4541.

53. Harrington, L. S.; Findlay, G. M.; Gray, A.; Tolkacheva, T.; Wigfield, S.; Rebholz, H.; Barnett, J.; Leslie, N. R.; Cheng, S.; Shepherd, P. R.; Gout, I.; Downes, C. P.; Lamb, R. F. The TSC1-2 tumor suppressor controls insulin-PI3K signaling via regulation of IRS proteins. *J Cell Biol.* **2004,** 166, 213-223.

54. Dibble, C. C.; Asara, J. M.; Manning, B. D. Characterization of Rictor phosphorylation sites reveals direct regulation of mTOR complex 2 by S6K1. *Mol Cell Biol.* **2009,** 29, 5657-5670.

55. Julien, L. A.; Carriere, A.; Moreau, J.; Roux, P. P. mTORC1-activated S6K1 phosphorylates Rictor on threonine 1135 and regulates mTORC2 signaling. *Mol Cell Biol.* **2010,** 30, 908-921.

56. Yang, H.; Rudge, D. G.; Koos, J. D.; Vaidialingam, B.; Yang, H. J.; Pavletich, N. P. mTOR kinase structure, mechanism and regulation. *Nature.* **2013,** 497, 217-223.

57. Krieger, E.; Darden, T.; Nabuurs, S. B.; Finkelstein, A.; Vriend, G. Making optimal use of empirical energy functions: force-field parameterization in crystal space. *Proteins.* **2004,** 57, 678-683.

58. Walker, E. H.; Pacold, M. E.; Perisic, O.; Stephens, L.; Hawkins, P. T.; Wymann, M. P.; Williams, R. L. Structural determinants of phosphoinositide 3-kinase inhibition by wortmannin, LY294002, quercetin, myricetin, and staurosporine. *Mol Cell.* **2000,** 6, 909-919.

59. Van Der Spoel, D.; Lindahl, E.; Hess, B.; Groenhof, G.; Mark, A. E.; Berendsen, H. J. GROMACS: fast, flexible, and free. *J Comput Chem.* **2005,** 26, 1701-1718.

60. Chaigne-Delalande, B.; Mahfouf, W.; Daburon, S.; Moreau, J. F.; Legembre, P. CD95 engagement mediates actin-independent and -dependent apoptotic signals. *Cell Death Differ.* **2009**.

FIGURE LEGENDS

Scheme 1. General synthesis of chromene derivatives.

Figure 1. Selection of new chromologs according to their ability to kill PI3K-addicted tumor cells and inhibit Akt phosphorylation. A. Representation of the first set of chromologs. **B.** The indicated compounds were incubated for 24 hours with leukemic T cell lines relying (CEM) or not (H9) on the PI3K signaling pathway for survival, and cell death was measured using an MTT viability assay. **C.** The 50% effective dose (ED_{50}) selectivity determined from data depicted in B. **D.** ***Upper panel:*** The PI3K-addicted T cell leukemia cell line CEM was incubated for 1 or 2 hours with 10 μM of the indicated chromologs. Cells were lysed, and the indicated immunoblots were performed. β-actin was used as a loading control. ***Lower panel:*** The immunoblots were assessed by densitometric analysis using ImageJ software, and the percentage of Akt phosphorylation was calculated using the following formula: [(phosphorylated Akt band intensity at time point x/intensity of whole protein band at time point x)/(intensity of P-Akt band at time zero/intensity of whole protein band at time point 0)]. **E.** ***Upper panel:*** The leukemic T cell line CEM was incubated with the indicated compounds for 24 hours, and cell death was measured by MTT viability assay. ***Lower panel:*** ED_{50} was assessed for each molecule using the MTT data depicted in the upper panel. **F.** CEM cells were incubated with the indicated chromologs (10 μM) for 1 or 2 hours. The cells were then lysed, and the indicated immunoblots were performed. Akt was used as a loading control. **G.** The percentage of Akt phosphorylation (P-Akt) was assessed as indicated in D. **H.** CEM cells were incubated with the indicated concentrations of chromologs for 2 hours. Cells were lysed, and the indicated immunoblots were performed. Akt was used as a loading control. **I.**

The percentage of Akt phosphorylation (P-Akt) was assessed as indicated in D, and the half maximal inhibitory concentration (IC_{50}) was determined for each chromolog.

Figure 2. Cytotoxic activity of different chromologs toward triple-negative, non-triple-negative, or HER2$^+$ breast cancer cell lines. A. A collection of cancer cell lines covering all types of breast cancers were incubated for 24 hours with the indicated chromologs, and cell death was measured by MTT viability assay. **B.** Table summarizing the ED_{50} of DHM25 against the breast cancer cell lines. Data are the means ± SEM of three different experiments.

Figure 3. DHM25 is a selective inhibitor of mTOR. A. DHM9 and DHM25 (1 μM) were tested by KinaseProfile assay to measure their inhibitory effect on 243 kinases. **B.** Using immunoblotting, the inhibitory effect of DHM25 and rapamycin on mTORC1 and mTORC2 activity was assessed by monitoring S6 and 4EB-P1 phosphorylation (for mTORC1) and Akt (Ser473) phosphorylation (for mTORC2). **C.** Comparison of the effects of DHM25 on mTOR activity. The amount of phosphorylation of the different substrates was quantified by densitometric analysis using ImageJ software and the following formula: [(phosphorylated band intensity at time point x/intensity of whole protein band at time point x)/(intensity of phosphorylated band at time 0/intensity of whole protein band at time point 0)].

Figure 4. The (*S*)-DHM25 enantiomer kills tumor cells and inhibits mTOR more efficiently than (*R*)-DHM25. A. Representation of the (*R*)- and (*S*)-DHM25 enantiomers. **B.** Leukemic cell lines reliant on PI3K signaling for survival (CEM and Jurkat cells) were incubated with the indicated chemicals for 24 hours, and cell death was measured by MTT viability assay. Data represent the means ± SEM of three independent experiments. **C.** CEM cells were incubated with the Indicated concentrations of (*R*)- and (*S*)-DHM25 for 2 hours.

Cells were lysed, and the indicated immunoblots were performed. Whole Akt and β-actin were used as loading controls. Data are representative of three independent experiments. **D.** Computer models for (*S*)-DHM25 and (*S*)-DHM9 in the catalytic pocket of human mTOR based on experimental structure PDBid 4JSN.

Scheme 2. Synthesis of DHM9 and DHM25 conjugated to different probes.

Figure 5. *In cellulo* analyses confirm that DHM25 is an mTOR inhibitor. A. DHM25 was conjugated with a biotin moiety. Models present the most representative structure of 60 ns molecular dynamics trajectories into the mTOR catalytic pocket (based on PDBid 4JSN) computed for DHM25 and its biotin-conjugated counterpart. **B.** MDA-MB-231 cells were pre-incubated with FITC alone or DHM25-FITC (10 μM) for 3 hours, fixed, and stained with anti-mTOR mAb. Images were analyzed by confocal microscopy (magnification, 40×). Data are representative of three independent experiments. **C.** CEM cells were incubated for 2 hours with the indicated concentrations of DHM25-biotin. Cells were lysed, and phosphorylation of Akt at serine 473 (mTORC2 substrate) was monitored by immunoblot. **D.** CEM cells were treated with 10 μM DHM25 alone or DHM25 conjugated to biotin for the indicated times, after which cells were lysed and the biotin moiety was pulled down with streptavidin-coated beads. Immunoprecipitates were subjected to an anti-mTOR immunoblot. **E.** CEM cells were treated for 2 hours with the indicated concentration of DHM25 or DHM9 conjugated to biotin. Cells were lysed, and the biotin moiety was pulled down with streptavidin-coated beads. Immunoprecipitates were subjected to an anti-mTOR immunoblot.

Figure 6. DHM25 is a covalent mTOR inhibitor. A. Models present the most representative structure of 60 ns molecular dynamics trajectories computed for DHM25 compounds into the

mTOR catalytic pocket (based on PDBid 4JSN). The lysine at position 2187 (K2187) is very close to the C4 atom of DHM25, suggesting a nucleophilic attack via a Michael addition leading to a covalent bond within the mTOR ATP pocket. **B.** CEM cells were incubated for 2 hours with 10 μM DHM25 or AZD8055. Then, cells were extensively washed and incubated for the indicated times in medium devoid of inhibitor. Cells were lysed, and phosphorylation of Akt at serine 473 (mTORC2 substrate) was monitored by immunoblot. **C.** DHM25 and its derivatives (DHM25-H2) in which the C3-C4 double bond was reduced. **D.** The indicated cells were treated for 16 hours with DHM25 or DHM25-H2, and cell death was evaluated by MTT assay. **E.** CEM cells were treated for 2 hours with the indicated concentration of DHM25 or DHM25-H2, and cells were lysed and the indicated immunoblots were performed. Data are representative of at least three independent experiments. **F.** The leukemic T cell lines CEM and Jurkat were incubated for 16 hours with the indicated concentration of DHM25 or its derivatives. Cell death was assessed by MTT assay. Data represent the mean ± SD of three independent experiments. Data represent the mean ± SD of three independent experiments. **G.** CEM cells were treated for 2 hours with the indicated concentrations of DHM25 or derivatives, and then the cells were lysed and the indicated immunoblots were performed. Data are representative of at least three independent experiments.

Scheme 3. Reduction of DHM25.

Scheme 4. Preparation of DHM25 analogs (variation of the EWG).

Figure 7. Non-toxic amounts of DHM25 inhibit cell migration in TNBC cells. A. TNBC cell lines (MDA-MB-231 and BT549) were incubated for 16 hours with the indicated concentration of DHM25. Cell death was assessed by MTT assay. Data represent the mean ±

SD of three independent experiments. **B.** TNBC cell lines were pre-incubated for 1 hour in the presence or absence of DHM25 (1 μM) and then treated with CD95L (100 ng/ml) for 24 hours. Cell migration was analyzed by Boyden chamber assay. Migrating Giemsa-stained cells were lysed, and absorbance was measured at a wavelength of 560 nm. Values represent the means ± SEM of three independent experiments. *$p < 0.05$, as calculated by two-tailed Mann–Whitney test. **C.** ***Upper panel:*** NSG mice injected with DHM25 (10 mg/kg) or with vehicle (control) were sacrificed 50 days after implantation of MDA-MB-231 xenografts. For each mouse, the primary tumor was harvested and weighed. ***$p < 0.0001$, as calculated by two-tailed Mann–Whitney test. ***Lower panel:*** Metastatic dissemination in the lungs of luminescent MDA-MB-231 tumor cells was evaluated in xenografted mice treated (+) or untreated (-) with DHM25 (10 mg/kg). For each mouse, lungs were harvested and the amount of invasive MDA-MB-231 cells was assessed by bioluminescence imaging (BLI). *$p < 0.05$, as calculated by two-tailed Mann–Whitney test. ***Inset:*** Lungs of xenografted mice analyzed by BLI.

Scheme 1

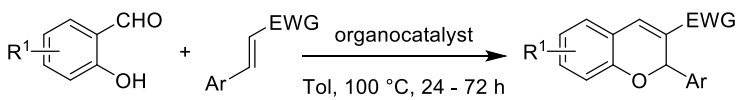

organocatalyst = pipecolic acid or 1,1,3,3-tetramethylguanidine

EWG = NO_2, CHO, $CONMe_2$, CO_2Me, CO_2H

Figure 1

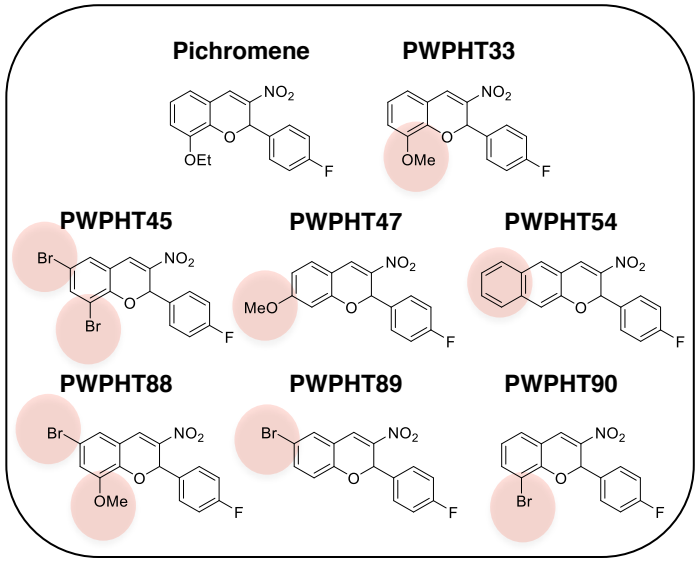

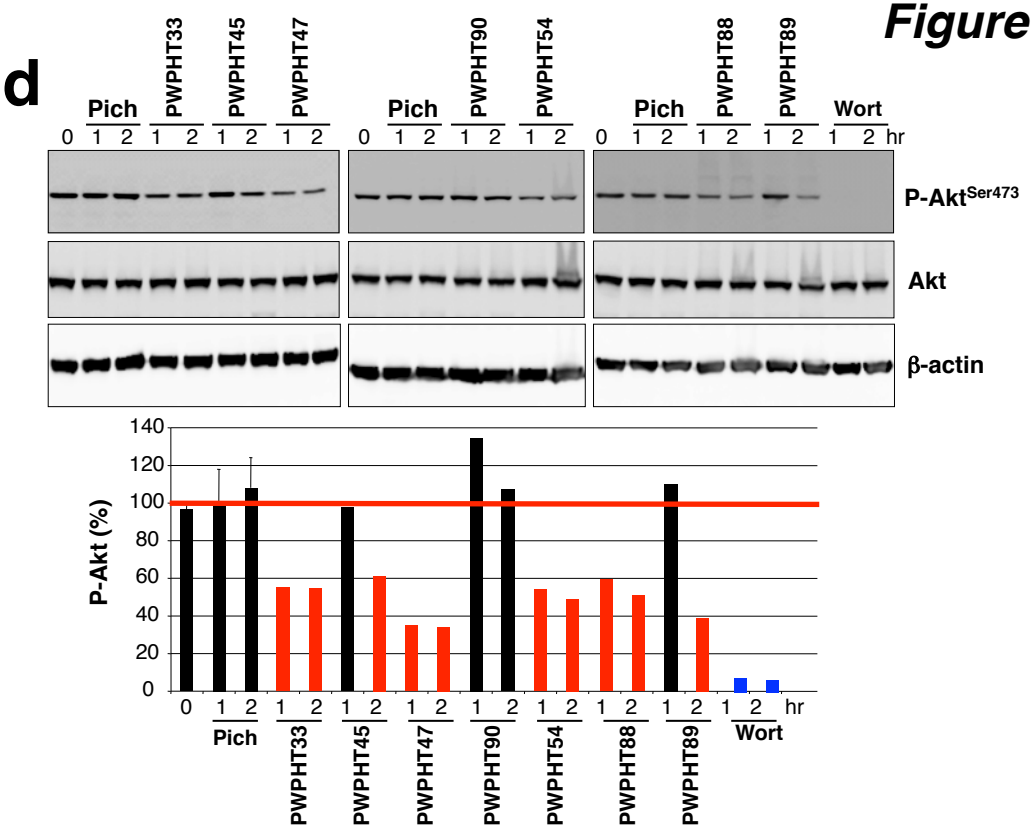

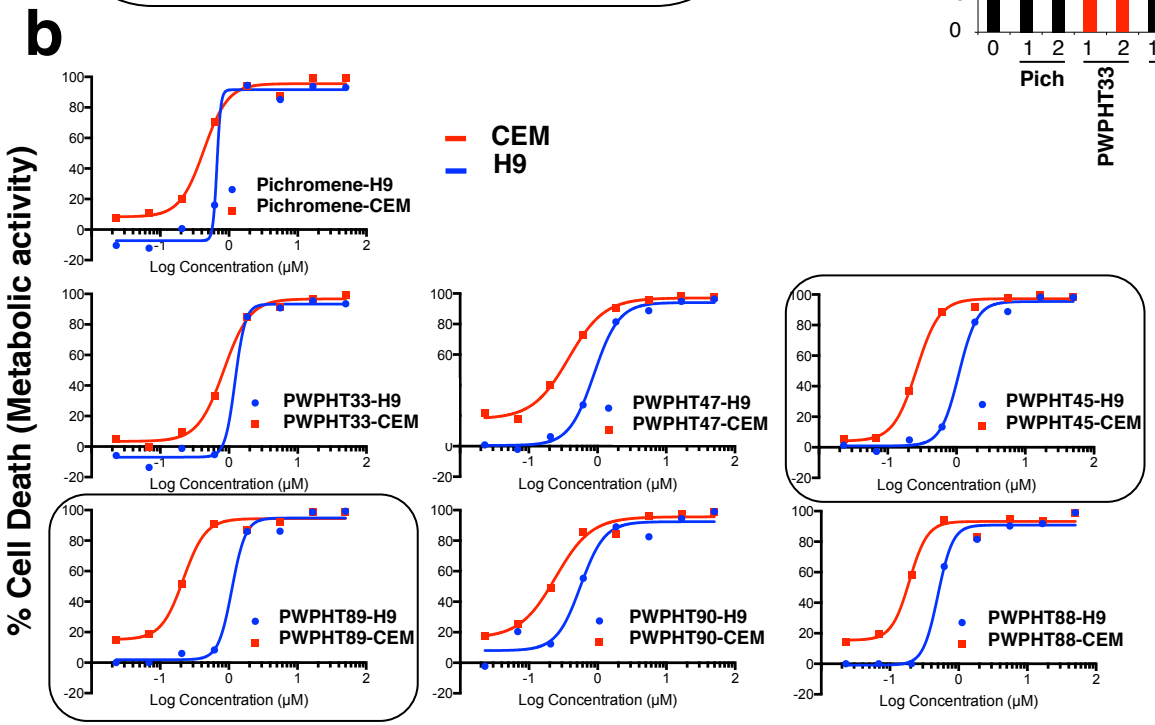

c

	H9 (EC_{50} (μM))	CEM (EC_{50} (μM))	Efficiency (ED_{50} Pich/PWPHT)	Selectivity (ED_{50} no-Addicted/addicted)
Pichromene	**0.666**	**0.430**	**1.000**	**1.549**
PWPHT33	1.229	0.842	0.511	1.460
PWPHT45	1.084	**0.262**	1.641	**4.136**
PWPHT47	0.891	**0.379**	1.136	2.353
PWPHT88	0.500	**0.193**	2.233	2.596
PWPHT89	1.111	**0.218**	1.973	**5.096**
PWPHT90	0.563	**0.244**	1.763	2.307

Figure 1

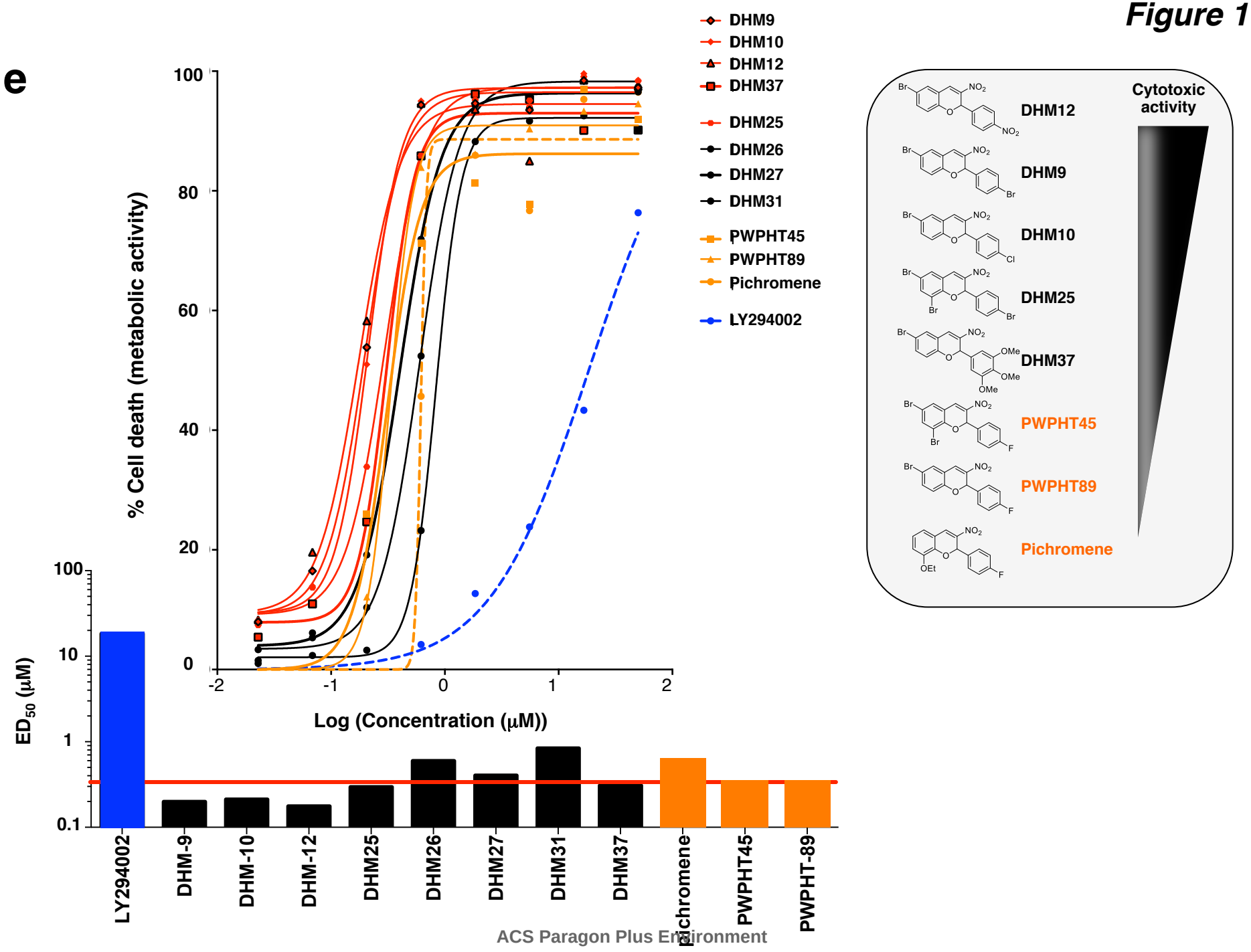

Figure 1

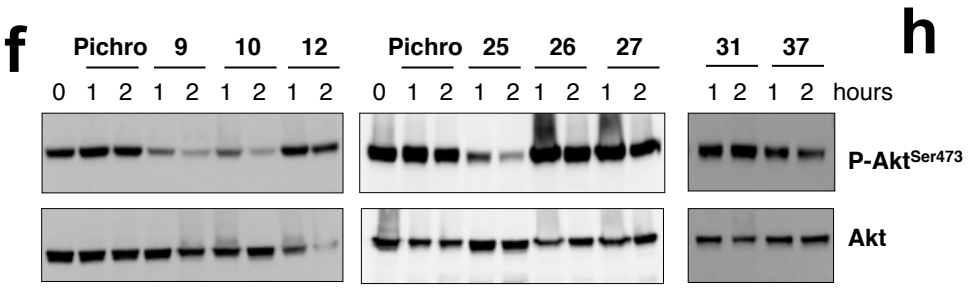

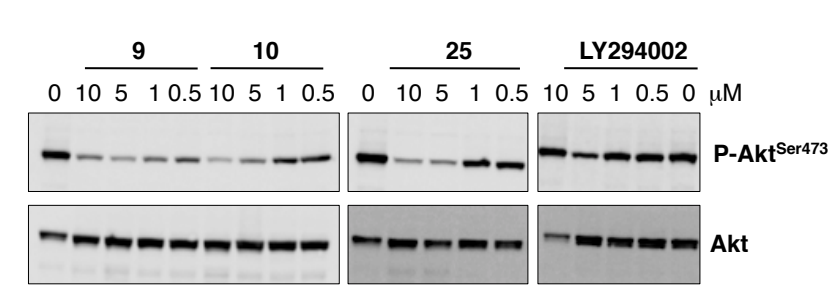

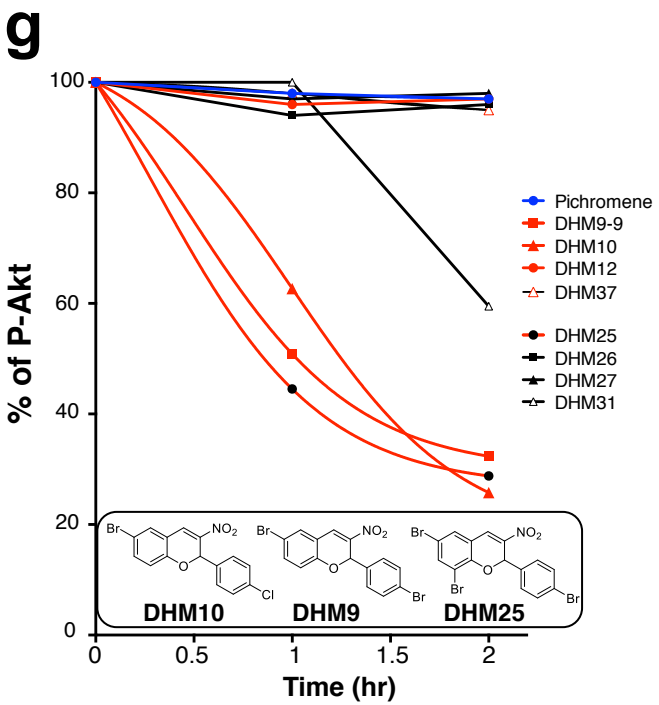

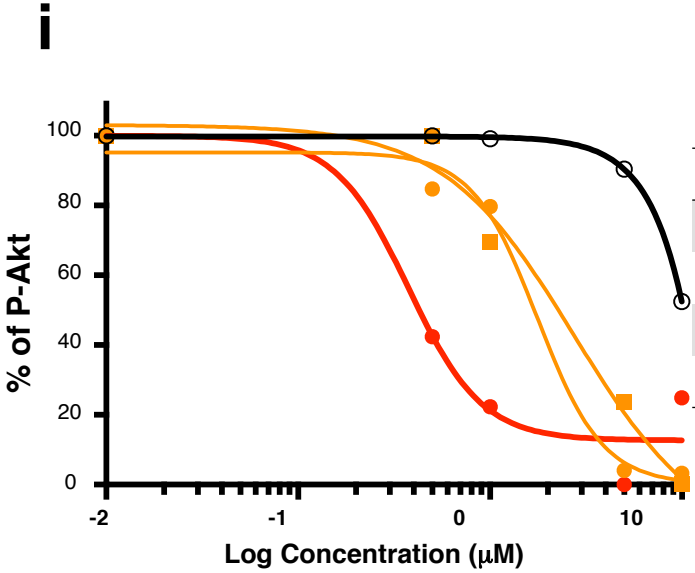

Molecule name	In cellulo IC50 (μM)
DHM9	0.376
DHM10	2.744
DHM25	1.768
LY294002	≥100

Figure 2

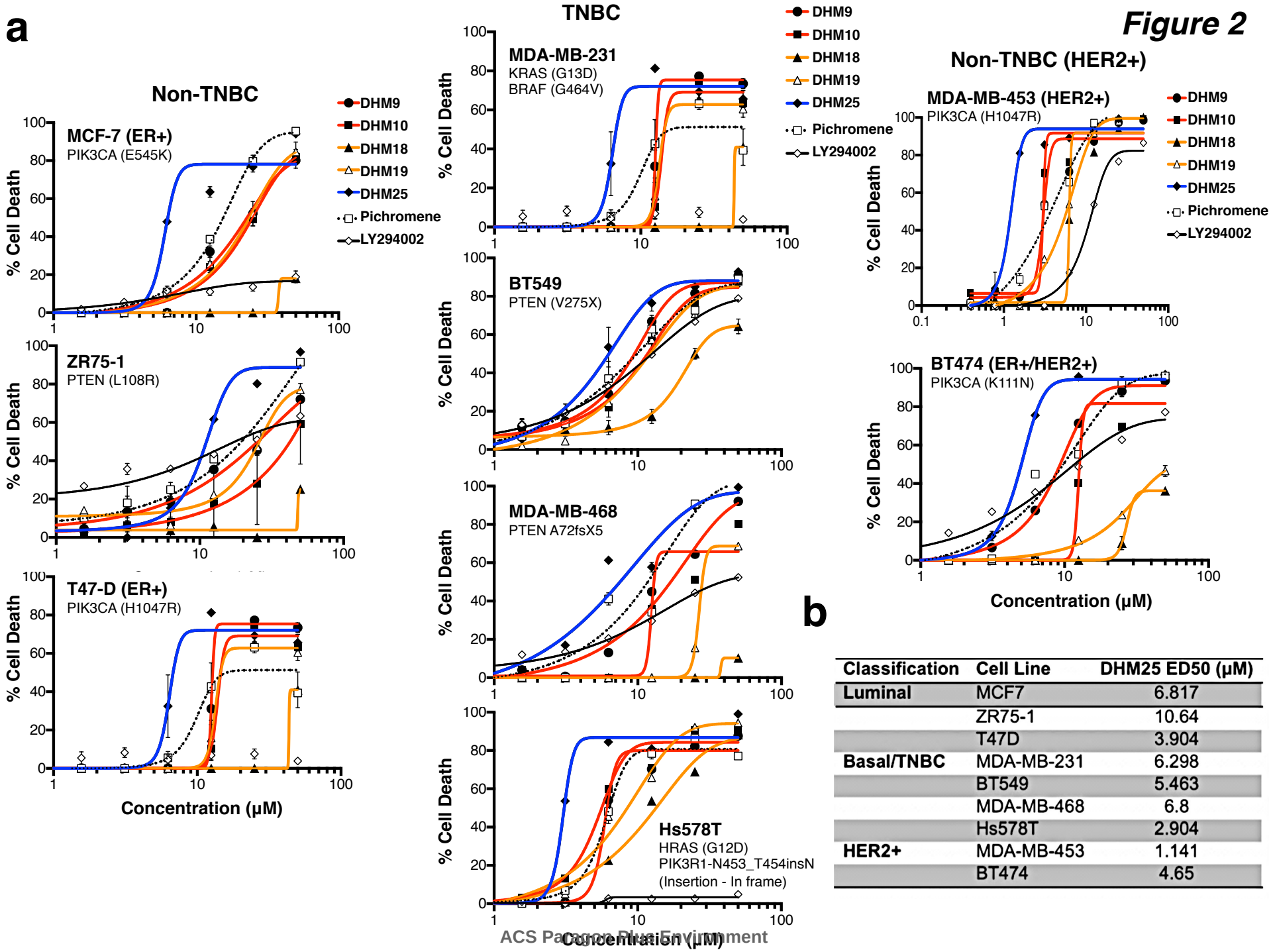

b

Classification	Cell Line	DHM25 ED50 (μM)
Luminal	MCF7	6.817
	ZR75-1	10.64
	T47D	3.904
Basal/TNBC	MDA-MB-231	6.298
	BT549	5.463
	MDA-MB-468	6.8
	Hs578T	2.904
HER2+	MDA-MB-453	1.141
	BT474	4.65

Figure 3

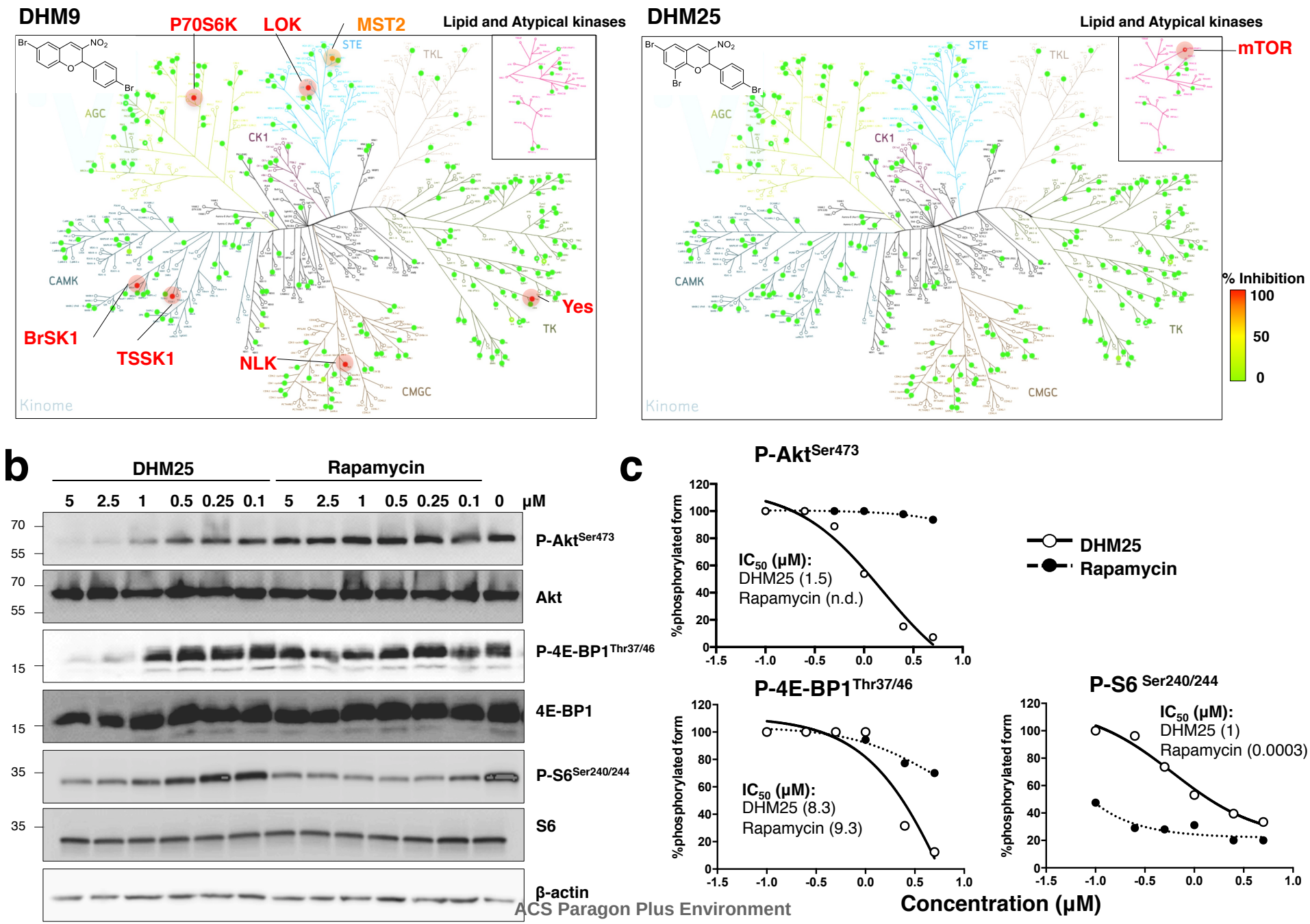

Figure 4

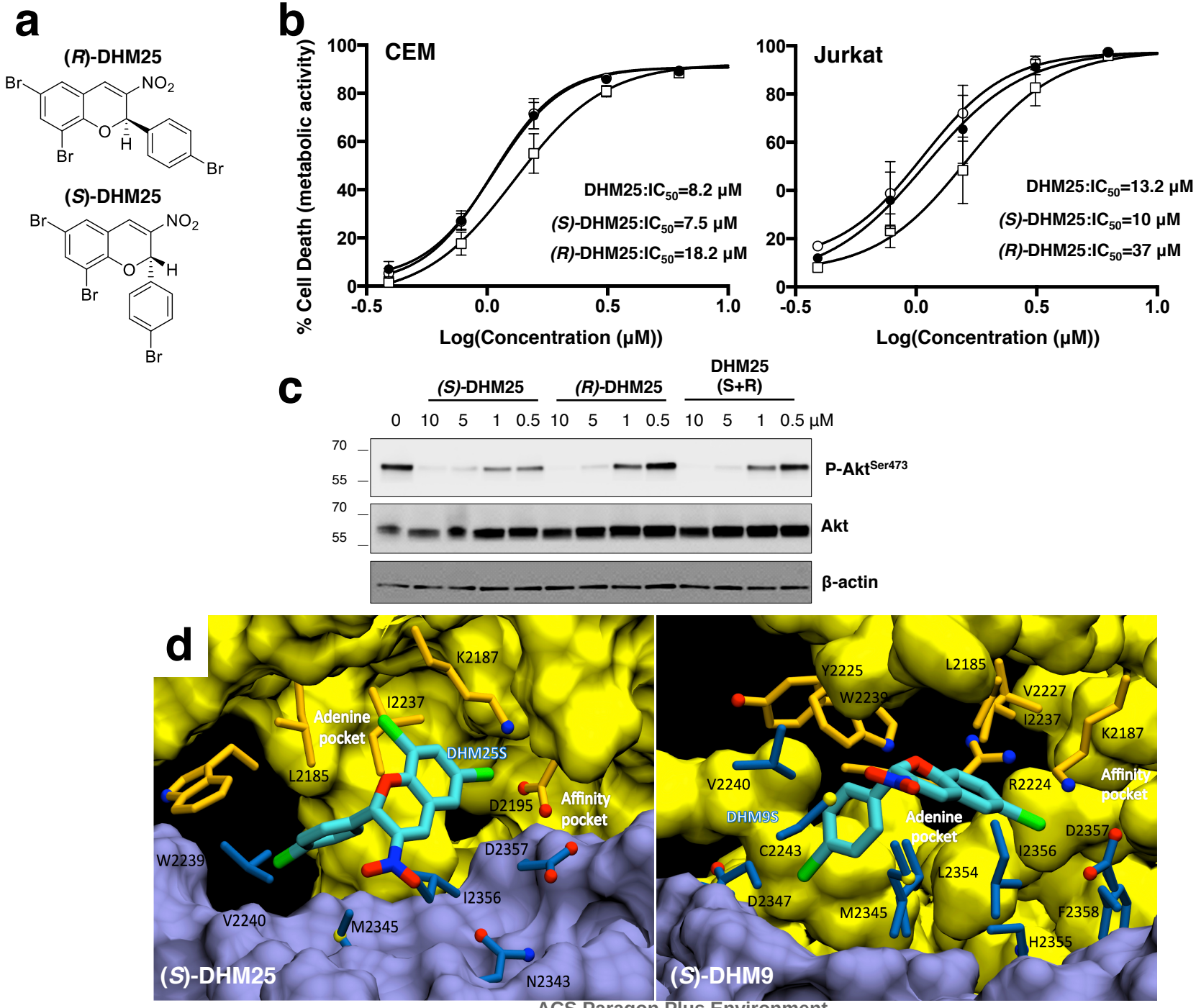
a
(R)-DHM25
(S)-DHM25
b
CEM
Jurkat
% Cell Death (metabolic activity)
Log(Concentration (μM))
DHM25:IC50=8.2 μM
(S)-DHM25:IC50=7.5 μM
(R)-DHM25:IC50=18.2 μM
DHM25:IC50=13.2 μM
(S)-DHM25:IC50=10 μM
(R)-DHM25:IC50=37 μM
c
(S)-DHM25
(R)-DHM25
DHM25 (S+R)
0 10 5 1 0.5 10 5 1 0.5 10 5 1 0.5 μM
P-AktSer473
Akt
β-actin
d
K2187
I2237
Adenine pocket
DHM25S
L2185
D2195
Affinity pocket
W2239
D2357
I2356
V2240
M2345
N2343
(S)-DHM25
Y2225
L2185
W2239
V2227
I2237
K2187
V2240
R2224
Affinity pocket
DHM9S
Adenine pocket
C2243
D2357
I2356
L2354
D2347
M2345
F2358
H2355
(S)-DHM9

Scheme 2

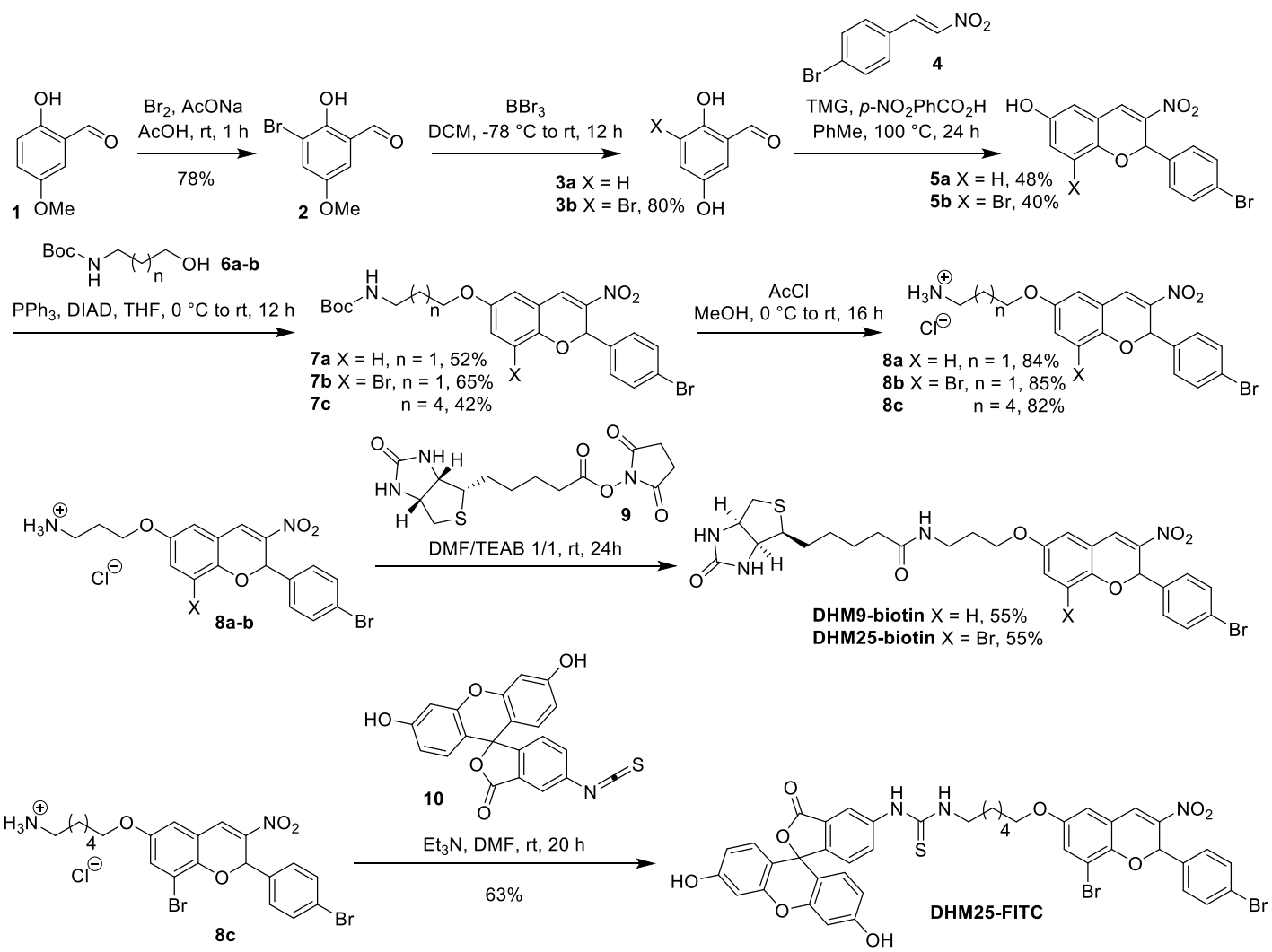
Br2, AcONa
AcOH, rt, 1 h
78%
BBr3
DCM, -78 °C to rt, 12 h
3a X = H
3b X = Br, 80%
TMG, p-NO2PhCO2H
PhMe, 100 °C, 24 h
5a X = H, 48%
5b X = Br, 40%
PPh3, DIAD, THF, 0 °C to rt, 12 h
7a X = H, n = 1, 52%
7b X = Br, n = 1, 65%
7c n = 4, 42%
AcCl
MeOH, 0 °C to rt, 16 h
8a X = H, n = 1, 84%
8b X = Br, n = 1, 85%
8c n = 4, 82%
DMF/TEAB 1/1, rt, 24h
DHM9-biotin X = H, 55%
DHM25-biotin X = Br, 55%
Et3N, DMF, rt, 20 h
63%
DHM25-FITC

Figure 5

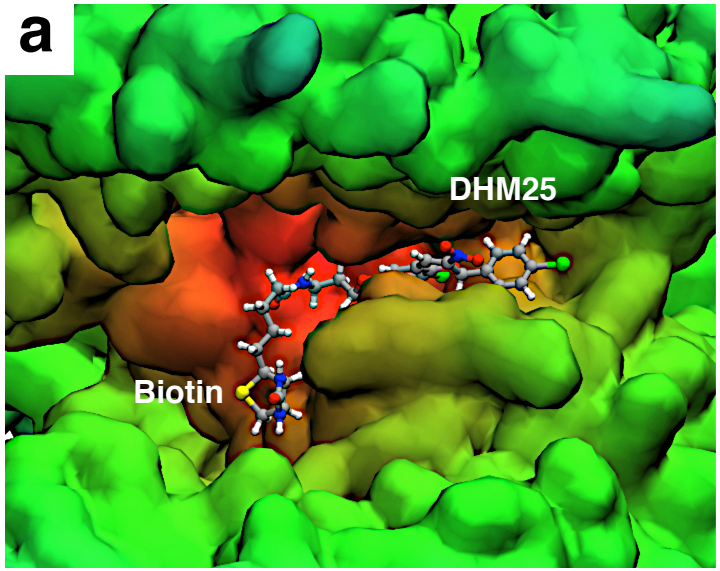

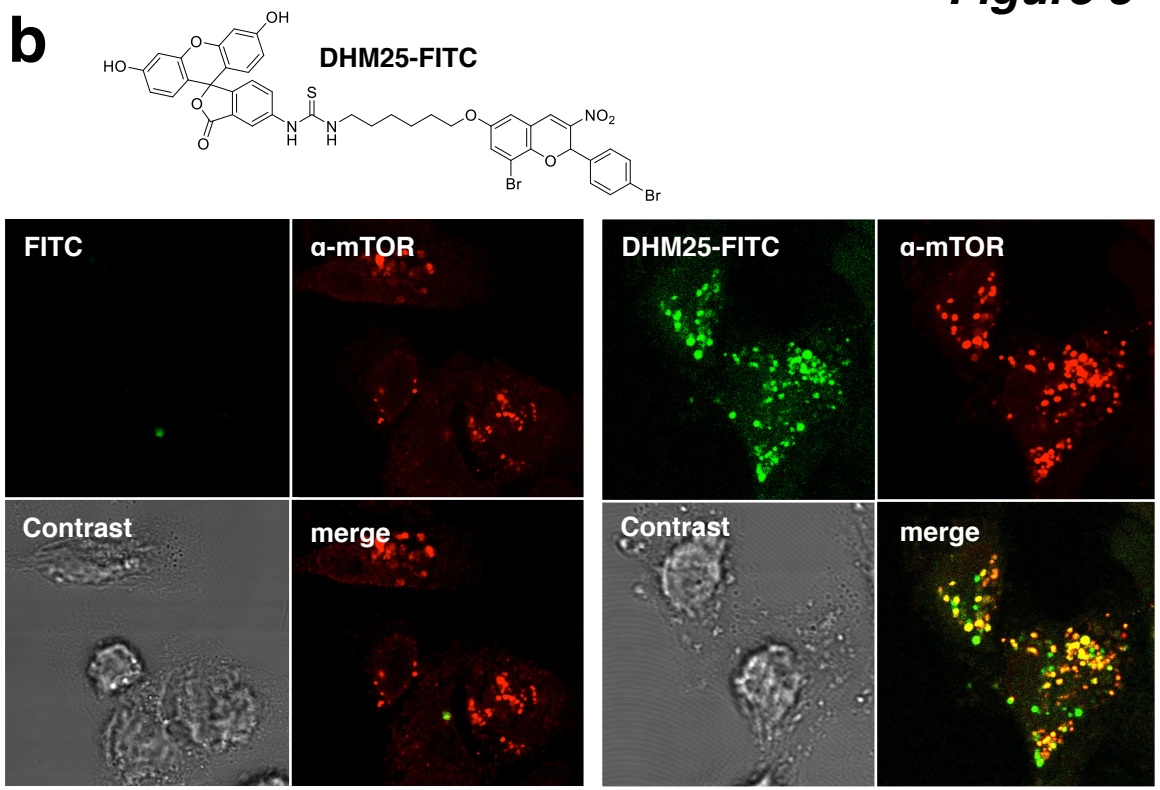

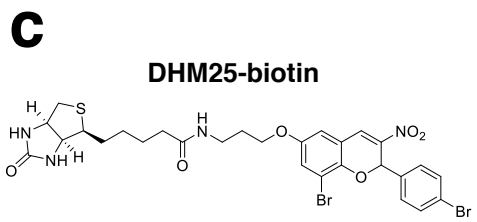

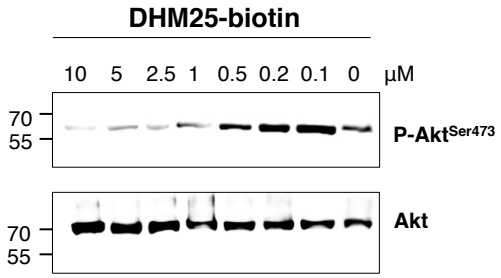

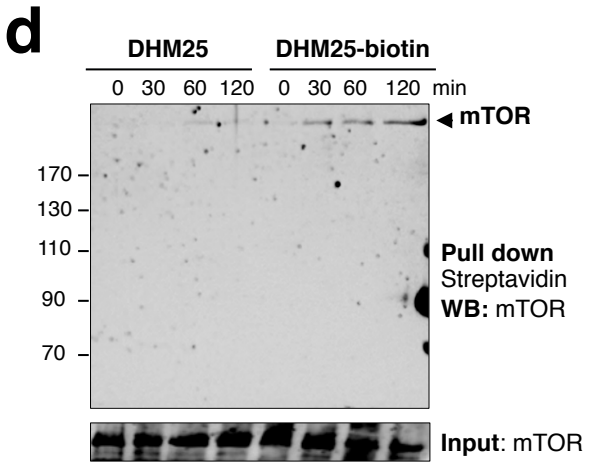

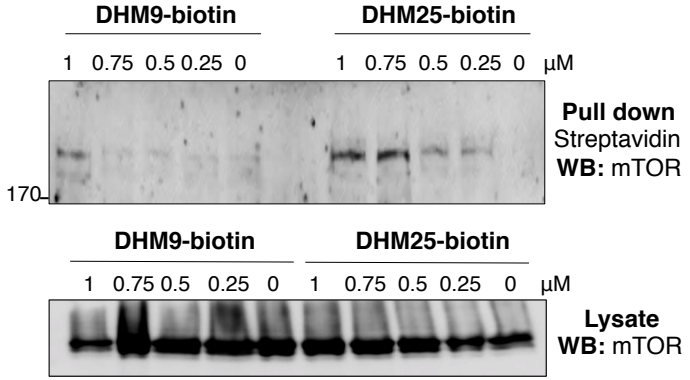

Scheme 3

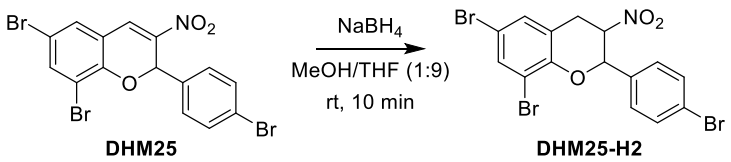

DHM25 **DHM25-H2**

Figure 6

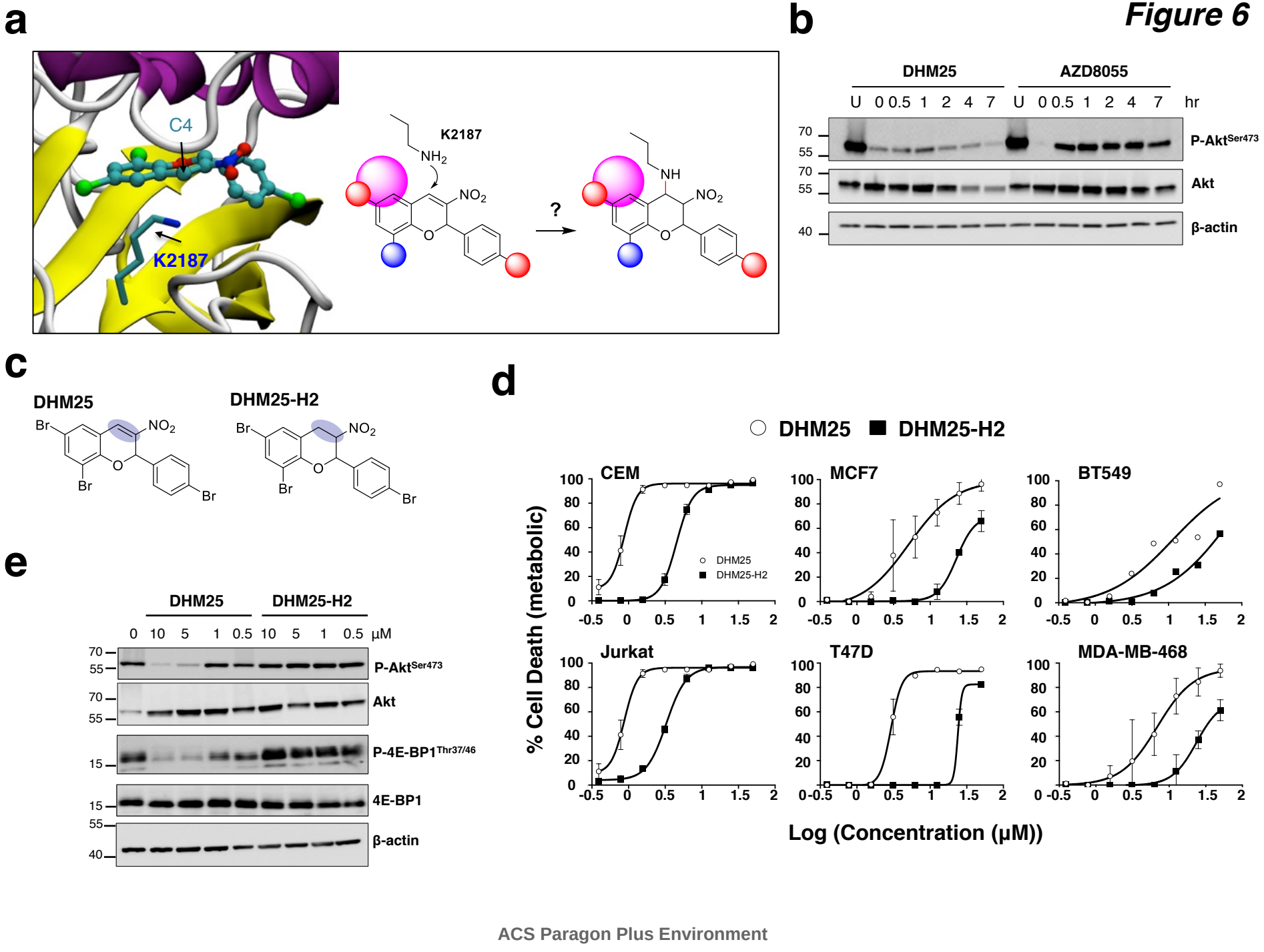
a
C4
K2187
K2187
NH2
NO2
?
NH
NO2
b
DHM25
AZD8055
U 0 0.5 1 2 4 7 U 0 0.5 1 2 4 7 hr
70
55
P-Akt Ser473
70
55
Akt
40
β-actin
c
DHM25
Br
NO2
Br
Br
DHM25-H2
Br
NO2
Br
Br
d
DHM25
DHM25-H2
CEM
MCF7
BT549
Jurkat
T47D
MDA-MB-468
% Cell Death (metabolic)
Log (Concentration (μM))
e
DHM25
DHM25-H2
0 10 5 1 0.5 10 5 1 0.5 μM
70
55
P-Akt Ser473
70
55
Akt
15
P-4E-BP1 Thr37/46
15
4E-BP1
55
40
β-actin

Scheme 4

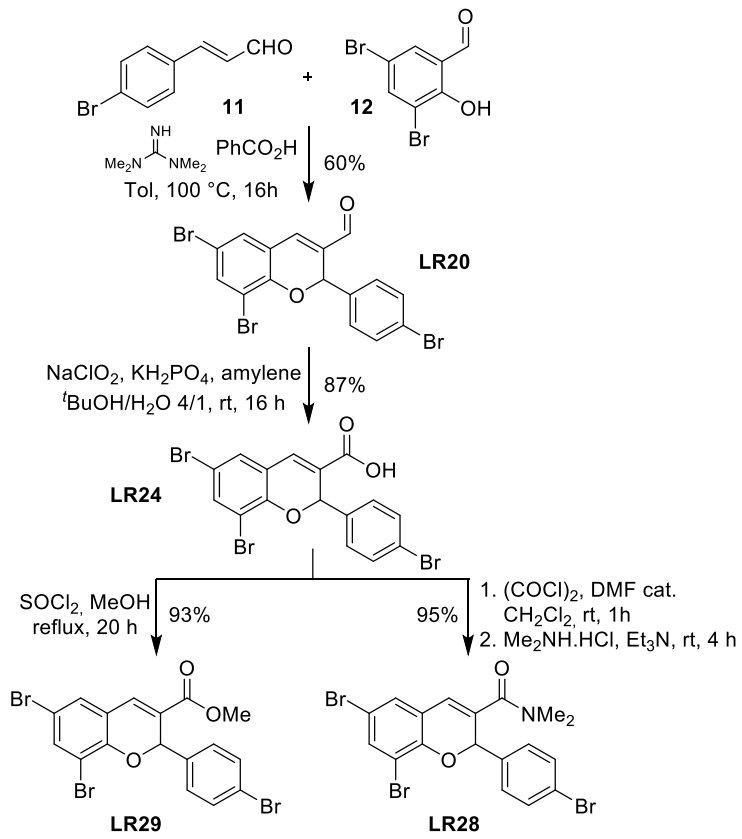
CHO
Br
11
+
Br
O
OH
Br
12
NH
Me2N
NMe2
PhCO2H
Tol, 100 °C, 16h
60%
O
Br
O
Br
Br
LR20
NaClO2, KH2PO4, amylene
tBuOH/H2O 4/1, rt, 16 h
87%
O
OH
Br
O
Br
Br
LR24
SOCl2, MeOH
reflux, 20 h
93%
95%
1. (COCl)2, DMF cat.
CH2Cl2, rt, 1h
2. Me2NH.HCl, Et3N, rt, 4 h
O
OMe
Br
O
Br
Br
LR29
O
NMe2
Br
O
Br
Br
LR28

Figure 6

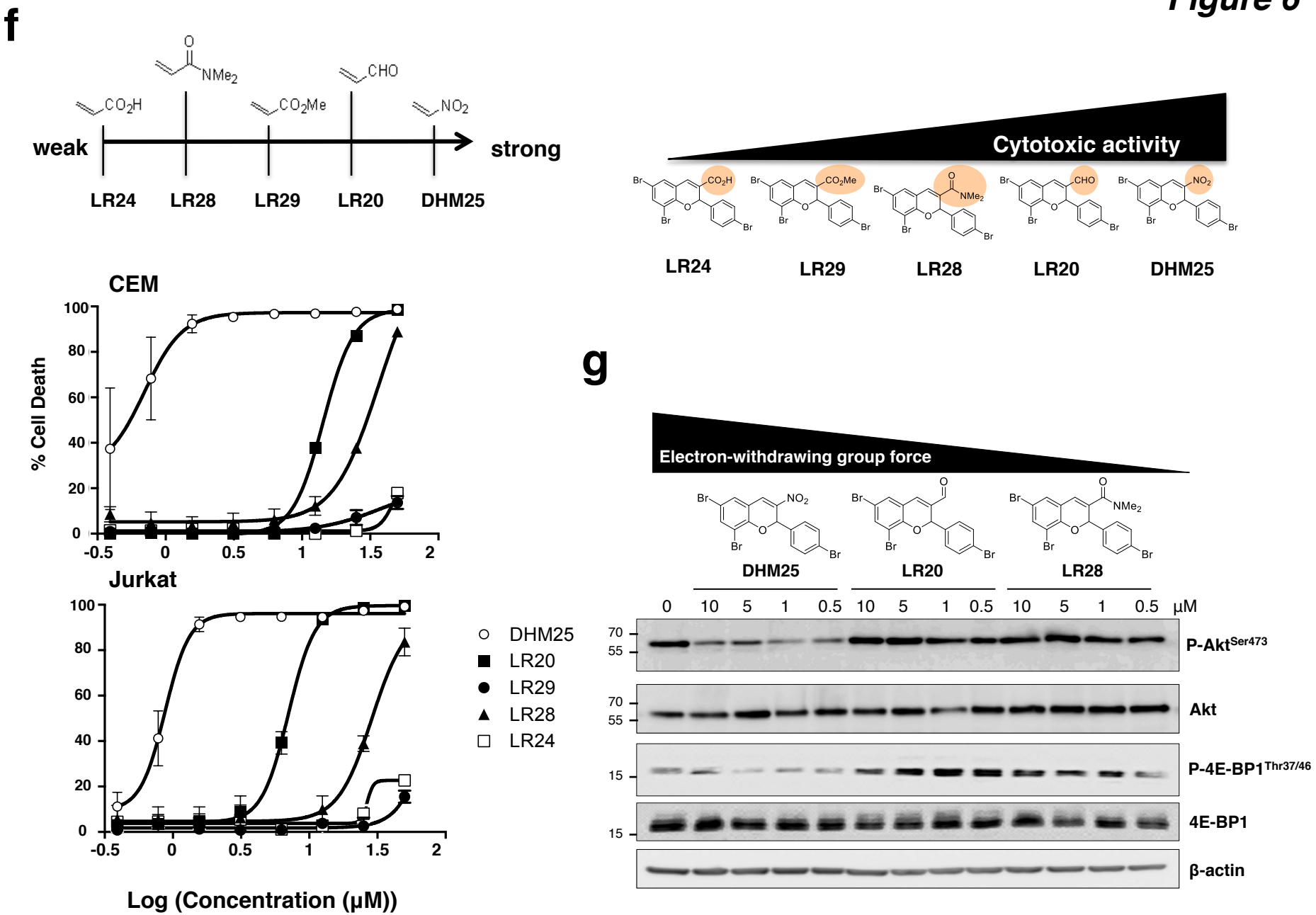
f
weak
strong
LR24
LR28
LR29
LR20
DHM25
Cytotoxic activity
LR24
LR29
LR28
LR20
DHM25
CEM
Jurkat
% Cell Death
Log (Concentration (μM))
DHM25
LR20
LR29
LR28
LR24
g
Electron-withdrawing group force
DHM25
LR20
LR28
0 10 5 1 0.5 10 5 1 0.5 10 5 1 0.5 μM
P-Akt Ser473
Akt
P-4E-BP1 Thr37/46
4E-BP1
β-actin

Figure 7

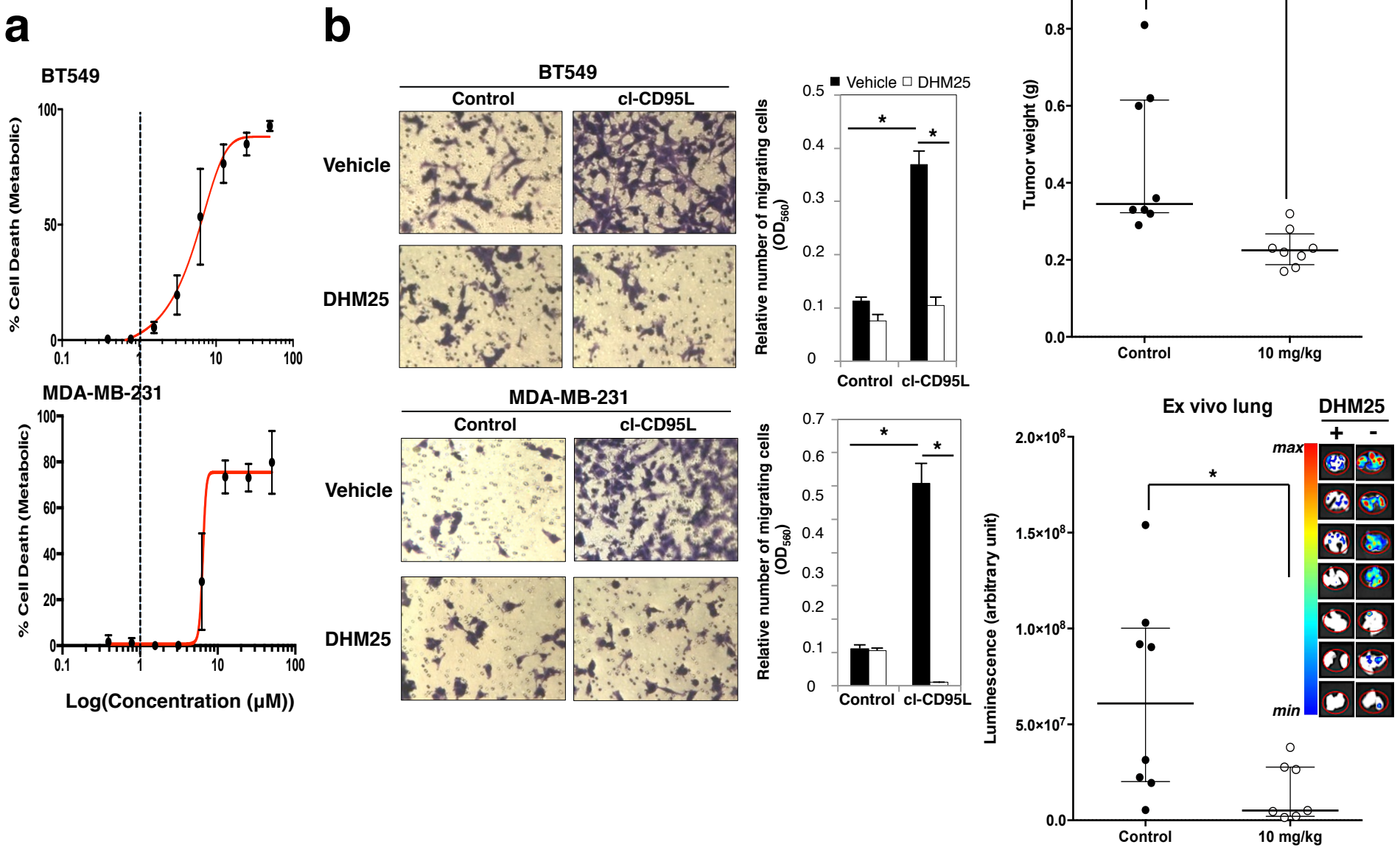
a
BT549
% Cell Death (Metabolic)
MDA-MB-231
% Cell Death (Metabolic)
Log(Concentration (μM))
b
BT549
Control
cl-CD95L
Vehicle
DHM25
Relative number of migrating cells (OD560)
Vehicle
DHM25
Control
cl-CD95L
MDA-MB-231
Control
cl-CD95L
Vehicle
DHM25
Relative number of migrating cells (OD560)
Control
cl-CD95L
c
Tumor weight (g)
***
Control
10 mg/kg
Ex vivo lung
DHM25
+
-
max
min
Luminescence (arbitrary unit)
*
Control
10 mg/kg